PLOS COMPUTATIONAL BIOLOGY

RESEARCH ARTICLE

Quantitative and Kinetic Proteomics Reveal ApoE Isoform-dependent Proteostasis Adaptations in Mouse Brain

Nathan R. Zuniga[1], Noah E. Earls[1], Ariel E. A. Denos[1], Jared M. Elison[1], Benjamin S. Jones[1], Ethan G. Smith[1], Noah G. Moran[1], Katie L. Broce[1], Gerome M. Romero[1], Chad D. Hyer[1], Kimberly B. Wagstaff[1], Haifa M. Almughamsi[2], Mark K. Transtrum[3], John C. Price[1]*

1 Department of Chemistry and Biochemistry, College of Computational, Physical, and Mathematical Sciences, Brigham Young University, Provo, Utah, United States of America, **2** Department of Chemistry, College of Science, Taif University, Taif, Saudi Arabia, **3** Department of Physics and Astronomy, College of Computational, Physical, and Mathematical Sciences, Brigham Young University, Provo, Utah, United States of America

* drjohncprice@gmail.com

Citation: Zuniga NR, Earls NE, Denos AEA, Elison JM, Jones BS, Smith EG, et al. (2024) Quantitative and Kinetic Proteomics Reveal ApoE Isoform-dependent Proteostasis Adaptations in Mouse Brain. PLoS Comput Biol 20(12): e1012407. https://doi.org/10.1371/journal.pcbi.1012407

Editor: Ivano Eberini, Università degli Studi di Milano, ITALY

Received: August 12, 2024

Accepted: November 3, 2024

Published: December 12, 2024

Data Availability Statement: The data generated in this investigation can be accessed via the ProteomeXchange Consortium via the PRIDE partner repository [118] (http://www.proteomexchange.org/) with the accession number PXD044460. The repository includes the raw LC-MS files used for both quantitative and kinetic files used in data analysis. In addition, Peaks Studio (Bioinformics Solutions Inc.) outputs containing peptide and protein level identification data for both quantitative and kinetic measurements are included in the repository. The output files from Deuterater

Abstract

Apolipoprotein E (ApoE) polymorphisms modify the risk of Alzheimer's disease with ApoE4 strongly increasing and ApoE2 modestly decreasing risk relative to the control ApoE3. To investigate how ApoE isoforms alter risk, we measured changes in proteome homeostasis in transgenic mice expressing a human ApoE gene (isoform 2, 3, or 4). The regulation of each protein's homeostasis is observed by measuring turnover rate and abundance for that protein. We identified 4849 proteins and tested for ApoE isoform-dependent changes in the homeostatic regulation of ~2700 ontologies. In the brain, we found that ApoE4 and ApoE2 both lead to modified regulation of mitochondrial membrane proteins relative to the wild-type control ApoE3. In ApoE4 mice, lack of cohesion between mitochondrial membrane and matrix proteins suggests that dysregulation of proteasome and autophagy is reducing protein quality. In ApoE2, proteins of the mitochondrial matrix and the membrane, including oxidative phosphorylation complexes, had a similar increase in degradation which suggests coordinated replacement of the entire organelle. In the liver we did not observe these changes suggesting that the ApoE-effect on proteostasis is amplified in the brain relative to other tissues. Our findings underscore the utility of combining protein abundance and turnover rates to decipher proteome regulatory mechanisms and their potential role in biology.

Author summary

We present a method to quantify and compare *in vivo* regulation of protein synthesis and degradation for thousands of individual proteins. Using this method, we compare the impact of ApoE isoforms which are known to bias the risk for Alzheimer's disease. We saw a pattern of changes that links together many published observations in a systematic way to identify biochemical trends increasing the risk of Alzheimer's disease.

software including turnover rate values are found within the repository while the code is found here (https://github.com/JC-Price/DeuteRater/releases). Lastly, the code used in the ontology analysis can be found by following this link to the GitHub repository (https://github.com/natepine/ApoE_Proteomics.git). The Python code used to analyze StringDB and calculate the FCs can be found in the GitHub repository JC-Price/PublicProteomeDataAnalysis: scripts for proteome data wrangling. https://github.com/JC-Price/PublicProteomeDataAnalysis.

Funding: This work was made possible by a grant from the Fritz B. Burns Foundation to JCP; the National Institutes of Health [R01AG066874] to JCP; Brigham Young University Undergraduate Research Awards to CDH, NEE, JME, NGM, EGS, KLB, KBW, and BSJ. A grant from Deanship of Scientific Research, Taif University to HA. The funders had no role in study design, data collection and analysis, decision to publish, or preparation of the manuscript.

Competing interests: The authors have declared that no competing interests exist

Introduction

Apolipoprotein E (ApoE) is one of the lipoproteins used for the transport of lipids and cholesterol throughout the body and the primary transporter in the brain. The three major subtypes of human ApoE—ApoE2, ApoE3, and ApoE4—differ by 2 amino acids and exhibit allelic frequencies of 8.4%, 77.9%, and 13.7%, respectively. [1,2] The ApoE3 allele is considered the normal or wild-type, and the behavior of the E2 or E4 isoforms differs in measurable ways. The ApoE2 protein isoform, characterized by an R158C substitution relative to the ApoE3, has been associated with decreased affinity for the LDL receptor [3,4], while the ApoE4 protein isoform, which features a C112R substitution relative to ApoE3, favors binding to very-low-density lipoprotein receptors [3,4]. Thus, these seemingly minor genotypic changes may lead to modified receptor mediated signaling, lipid availability and metabolic function, or a combination of factors.

Both ApoE2 and E4 modulate disease risk relative to ApoE3. For example, Ferrer et al. [5] observed a ~5-fold increase in Alzheimer's Disease (AD) prevalence in carriers of the ApoE4 allele relative to ApoE3 carriers and a decreased risk (~0.5 fold) in individuals expressing the ApoE2 allele. Although ApoE2 expression protects against AD, its expression is associated with the increased incidence of familial type III hyperlipoproteinemia—a disorder characterized by an inability to metabolize lipids including cholesterol and triglycerides.[6] ApoE isoforms have also been implicated in the development of Parkinson's disease [7], vascular pathology [8], and most recently, COVID-19 prognosis[9].

Some mechanistic details have been identified for how the ApoE alleles modulate an individual's risk for disease. ApoE is a transporter of amyloidβ [10–13], a widely recognized biomarker in AD development. ApoE-isoforms modulate brain mRNA expression, presumably in response to changes in lipid availability[14] as well as direct transcriptional effects.[15] Here we used both quantitative and kinetic proteomics to explore the impact of human ApoE genotypes in the proteome of mice (Fig A in S1 File). Both approaches leverage liquid chromatography and mass spectrometry (LC-MS) to identify and quantify thousands of proteins (Fig 1A). We apply a simplified kinetic model of proteostasis (Figs 1B and B in S1 File) combining turnover rate and concentration data to reveal ApoE isoform-dependent regulation of protein synthesis and degradation. We investigated the liver and brain, because there is strong evidence that of the ~16 major apolipoproteins, only ApoA1 can cross the blood brain barrier. [16] So although chemically identical, ApoE is found in two separate pools. The brain produces its own ApoE using astrocytes [4,17], whereas ApoE for the rest of the body is produced in the liver by hepatocytes [8,18]. Our analysis identifies key brain-specific proteostasis changes, as evidenced by pathway-level differences in synthesis and degradation. Building upon a significant body of literature and this proteome scale study, we propose a unifying mechanism wherein ApoE alleles systemically impact cellular proteostasis through alterations in endosomal trafficking, mitochondrial function, and proteo-lysosomal activity.

Results

Proteome ontology analysis

In our analysis, we identified 4,849 proteins in the brain tissue across the three ApoE-isoform groups (n = 47). From these, we determined protein abundance and turnover rate FCs for comparisons: ApoE2 vs. ApoE3 (E2vsE3) and ApoE4 vs. ApoE3 (E4vsE3). Here, ApoE3 serves as the reference 'normal' control. We quantified 3,532 abundance FCs for both the E2vsE3 and E4vsE3 comparisons (S2 and S3 Tables). With a smaller number of turnover rate FCs 1,430 for E2vsE3 and 1,405 FCs for E4vsE3 because of the more rigorous statistical filtering criteria.

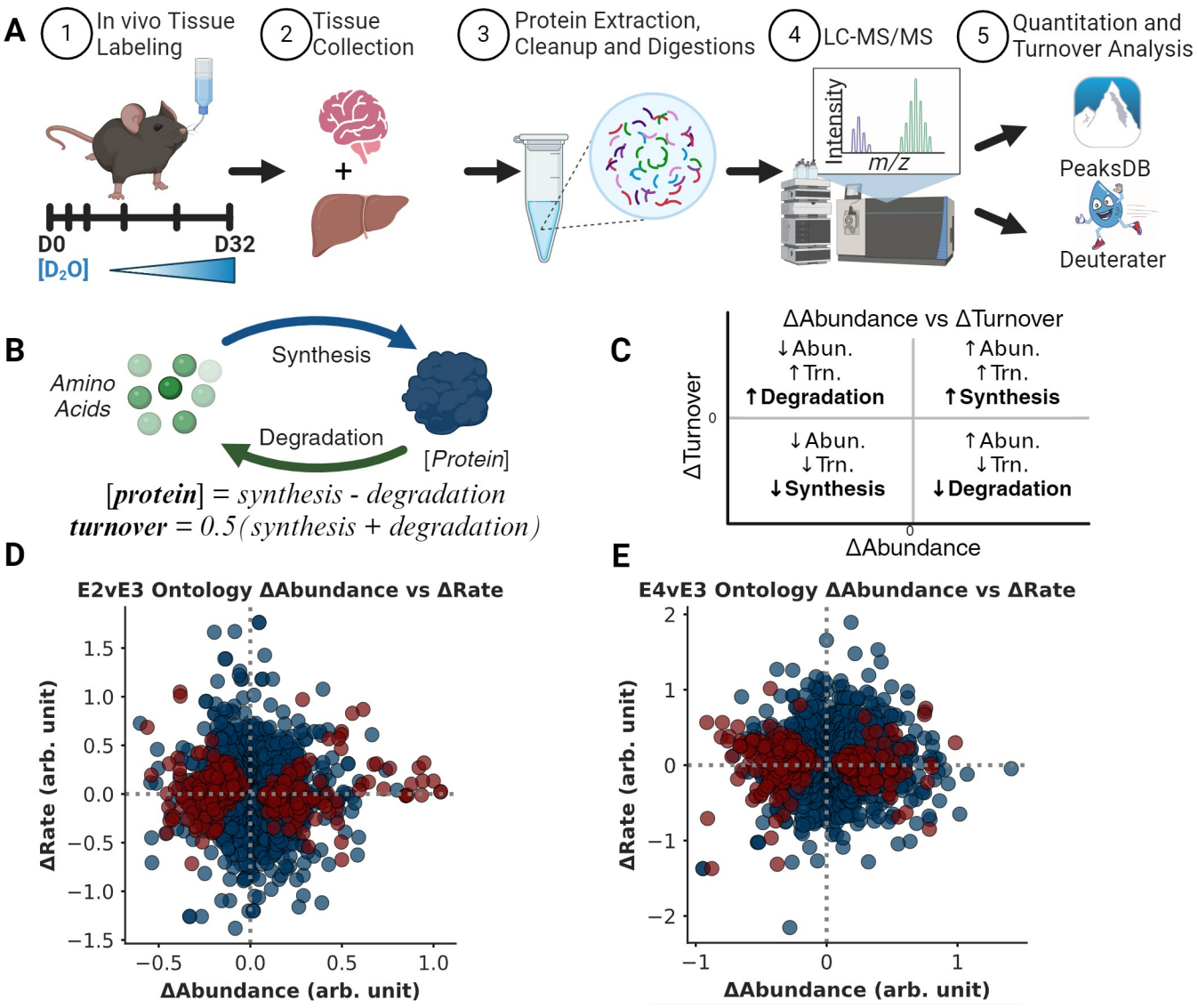

Fig 1. Quantifying ApoE-dependent proteome regulation **A.** Homozygous ApoE transgenic mice (ApoE2, E3, or E4, n = 24 each) were given 8% D2O drinking water for up to 32 days. Peaks Studio (Bioinformatics Solutions Inc.) was used for peptide-protein identification (IDs) and quantitation while Deuterater software was used for turnover rate calculation. **B.** A simple proteostasis model relates protein abundance ([protein]) and turnover rates to in vivo synthesis and degradation. **C.** Regulation of synthesis and degradation can be inferred from Δabundance (x-axis) and Δturnover (y-axis) and visualized using a proteostasis plot. **D & E.** Proteostasis plot showing 276 and 288 protein ontologies with significant Δabundance (red circles) in ApoE2 (panel D) and ApoE4 (panel E)mice relative to ApoE3 mice (E4vsE3) (BH-PV < 0.05). Created with Matplotlib.py, Plotly.py, Biorender and InkScape.

https://doi.org/10.1371/journal.pcbi.1012407.g001

We focused on ontologies from six databases: *GO Function*, *GO Component*, *GO Process*, *WikiPathways*, *Reactome*, and *KEGG*. We calculated the average abundance FC (Δabundance) and turnover rate FC (Δturnover) for the proteins observed in each ontology (Please refer to the *Ontology-level Calculations* in the methods section). This yielded ~2700 ontology-level comparisons of average Δabundance and Δturnover calculations for both E2vsE3 and E4vsE3 (S4 Table). The interpretation (Fig 1C) relies on the traditional understanding of protein turnover, contextualizing changes in protein expression. It offers a lens to assess the variances in the steady states of ApoE genotypes [19]. Using a one-sample t-test, we discerned which ontologies deviated significantly from a median Δabundance of 0. In the E2vsE3 comparison, we

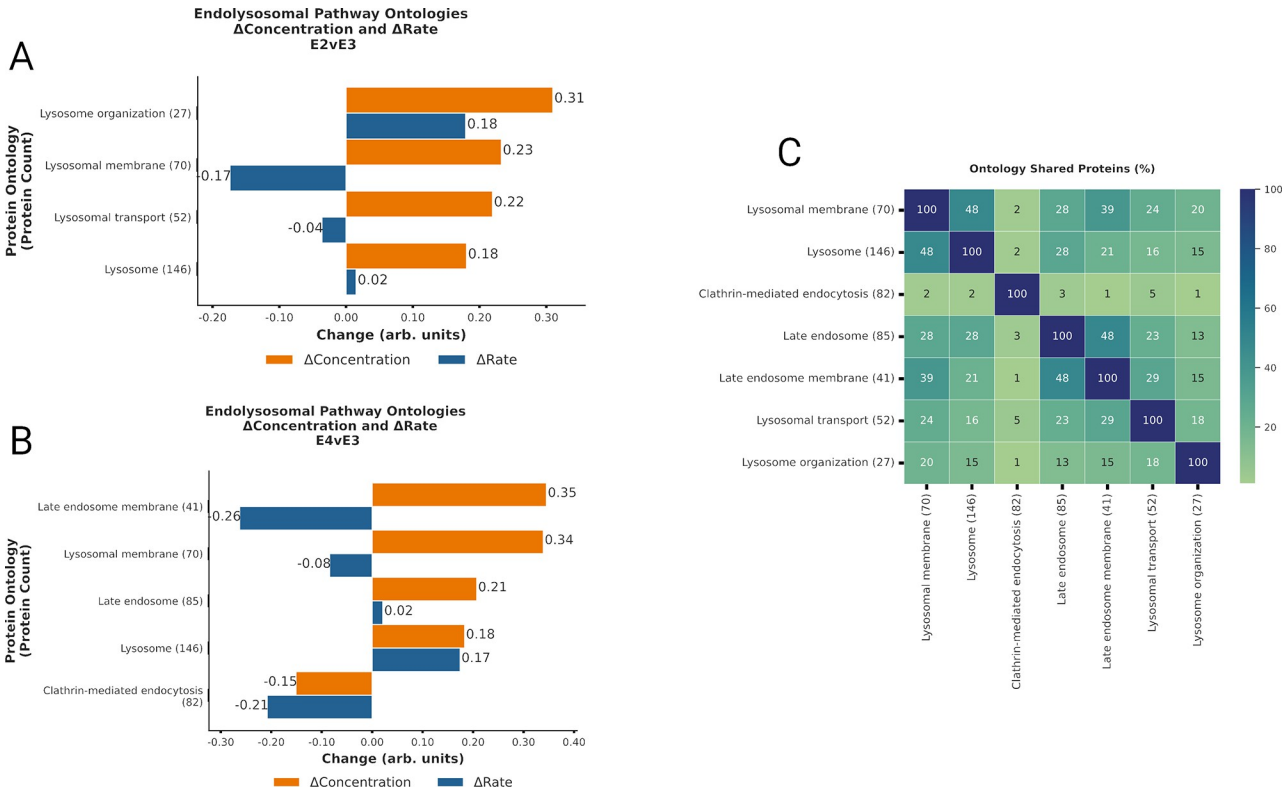

Fig 2. ApoE4 expression disrupts endosomal maturation and ApoE2 increases lysosomal capacity. A-B. Bar plot displaying Δabundance (orange) and Δturnover (blue) of proteins detected in all experimental cohorts for significant* ontologies related to endolysosomal trafficking in the E2vsE3 comparison (A) and in the E4vsE3 comparison (B). **C.** Heatmap displaying % of proteins shared across the endolysosomal ontologies with significant* Δabundance. *(*BH-PV < 0.05)*. Created with Matplotlib.py and InkScape.

https://doi.org/10.1371/journal.pcbi.1012407.g002

identified 284 protein ontologies with notable Δabundance (BH-PV < 0.05) (Fig 1D). For the E4vsE3 comparison, 287 protein ontologies had significant Δabundance (BH-PV < 0.05) (Fig 1E).

The box plots in Figs 2–5 summarize the Δabundance and Δturnover for ontologies with significant Δabundance shifts. To maximize visibility and to accommodate for space limitations, these boxplots do not contain outlier points but Figs C-F in S1 File contain outlier points. Given that some ontologies are repetitive, proteins depicted in the box plots might appear in multiple ontologies with analogous names/functions. When faced with such redundancies, we typically chose the ontology with superior coverage (Observed/Total) for representation. As a convention, each ontology is presented in an "*ontology name (n)*" format, where (n) indicates the count of quantified proteins within that ontology. Overlap between similar ontologies is shown in the heatmap.

ApoE Isoforms Modulate Synthesis and Degradation of Endocytic Vesicle Components

We observed that multiple ontologies with significant Δabundance were associated with endocytosis and vesicular processing (Fig 2). Specifically, the general *Endocytosis (158)* ontology demonstrated increased Δabundance and decreased Δturnover, suggesting reduced degradation in both ApoE2 and ApoE4 compared to ApoE3. In the context of ApoE2, *Clathrin-mediated endocytosis (82)*, *Clathrin binding (35)*, and *Clathrin coat (26)* mirrored the same

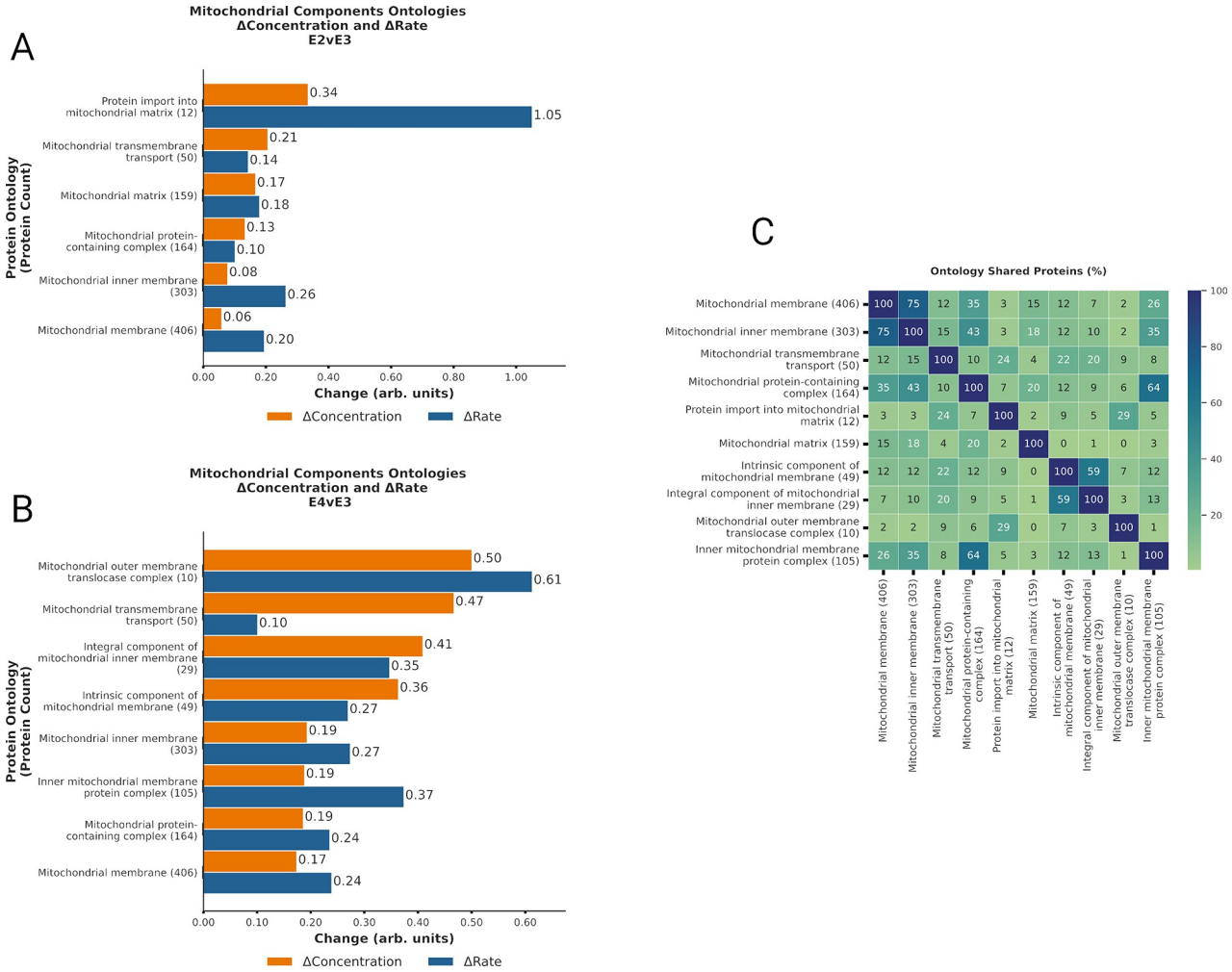

Fig 3. ApoE genotype differentially regulates mitochondrial proteostasis. A-B. Bar plot displaying Δabundance (orange) and Δturnover (blue) for ontologies of proteins detected in all experimental cohorts related to mitochondrial components with significant* Δabundance in the E2vsE3 comparison (A) and in the E4vsE3 comparison (B). **C.** Heatmap displaying % of proteins shared across the mitochondrial ontologies with significant* Δabundance. ***(*BH-PV** $<$ **0.05)***. Created with Matplotlib.py and InkScape.

https://doi.org/10.1371/journal.pcbi.1012407.g003

↓degradation effect observed in endocytosis, while *SNARE complex (32)* showed diminished Δabundance and Δturnover, suggesting a decline in protein synthesis compared to ApoE3. Moreover, ApoE2 expression led to significant alterations in several regulatory ontologies tied to endocytosis and vesicular processes, such as: *Endocytic recycling (34)* (↑synthesis), *Early endosome* (↑synthesis), and *Regulation of endocytosis (15)* (↑synthesis). In ApoE2, proteins related to *Lysosome Vesicle Biogenesis (18)* have lower degradation while *Regulation of Endocytosis (107)* had increased synthesis leading to higher abundance of these protein groups and presumably more efficient endolysosomal function.

In both ApoE2 (E2vsE3) and ApoE4 (E4vsE3) we noted less degradation of general *lysosome (146)* proteins. Within this general ontology, the *lysosomal membrane (70)* ontology had diminished Δabundance and Δturnover only in the ApoE4 group, suggesting less synthesis of the membrane components compared to ApoE3. This is consistent with large lysosomal vesicles stored in ApoE4 cells [13,20]. In ApoE4 mice there was higher Δabundance and Δturnover (↑synthesis) of *Phosphatidylinositol binding (90)* relative to ApoE3. Conversely, there was a

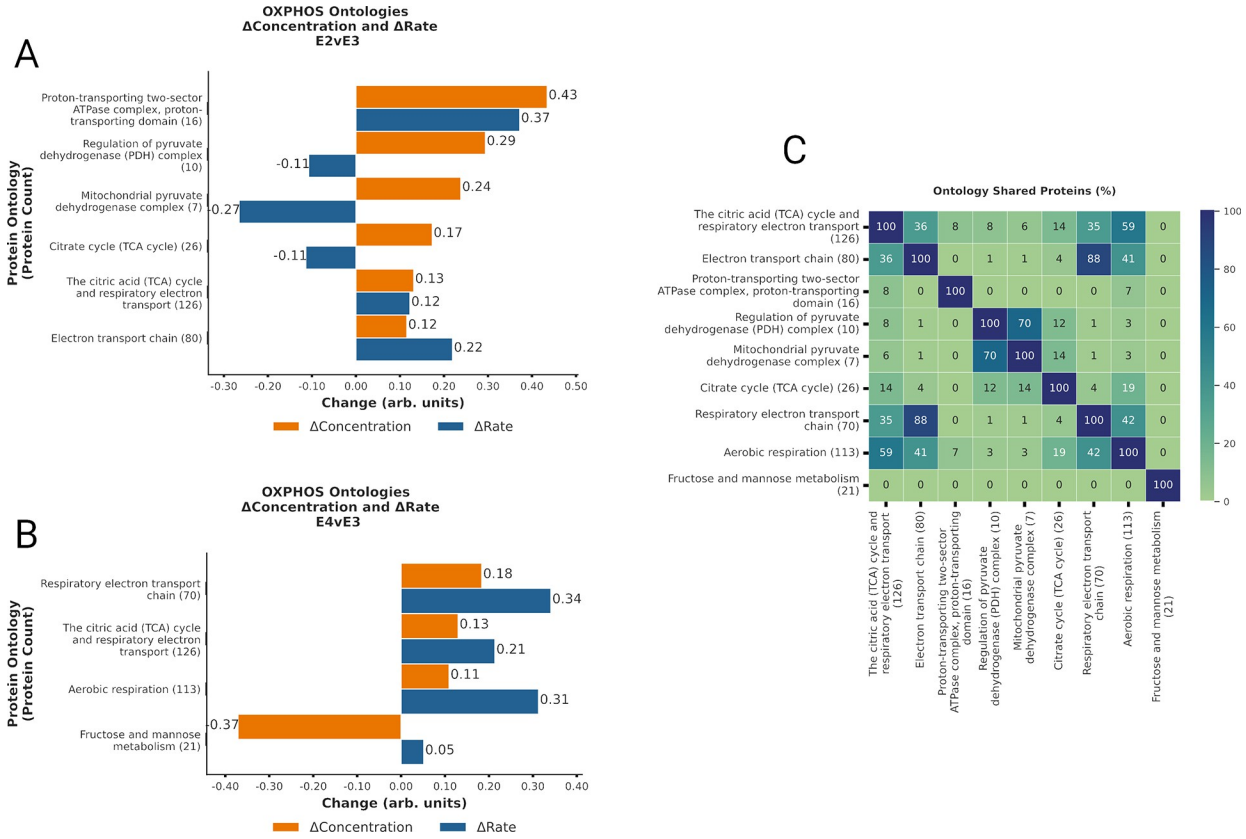

Fig 4. ApoE2 and ApoE4 expression drive changes in cellular fuel selection **A-B.** Bar plot displaying Δabundance (orange) and Δturnover (blue) for ontologies of proteins detected in all experimental cohorts belonging to oxidative phosphorylation with significant* Δabundance in the E2vsE3 comparison (A) and in the E4vsE3 comparison (B). **C.** Heatmap displaying % of proteins shared across the oxidative phosphorylation ontologies with significant* Δabundance. ***(*BH-PV** $<$ **0.05)***. Created with Matplotlib.py and InkScape

https://doi.org/10.1371/journal.pcbi.1012407.g004

decline in both Δabundance and Δturnover (↓synthesis) of *SNARE interactions in vesicular transport (19)*, *Synaptobrevin 2-SNAP-25-syntaxin-1a complex (5)*, and *SNARE complex (32)*.

ApoE isoforms modulate synthesis and degradation of mitochondrial components

Our analysis identified significant Δabundance (BH-PV $<$ 0.05) changes for multiple ontologies related to mitochondrial components (Fig 3). In the E4vsE3 comparison, these ontologies included mitochondrial membranes, protein transport, and morphology (Figs 3A and C in S1 File). Each of these ontologies displayed a negative Δabundance coupled with a positive Δturnover, signifying ↑degradation. We also detected ↓synthesis of *mitochondrial calcium ion transmembrane transport (12)* and *mitophagy (18)*. In contrast, ApoE4 *mitochondrial matrix (159)* also had ↑degradation. (Figs 3B and C in S1 File) The percentage of overlapping proteins in each mitochondrial component ontology is displayed in Fig 3C. The key finding from these ontologies is that within the ApoE2 mice there is a coherent increase in the degradation of all mitochondrial components consistent with an increase in mitochondrial degradation as an entire unit. In contrast, the ApoE4 tissues show discordant changes in matrix versus membrane proteins suggesting that mitochondrial maintenance is more piecemeal and that mitophagy may be less efficient as previously suggested in the literature [21]. Both the ApoE2 and the ApoE4 results are synergistic with the changes in lysosome dynamics discussed above. In

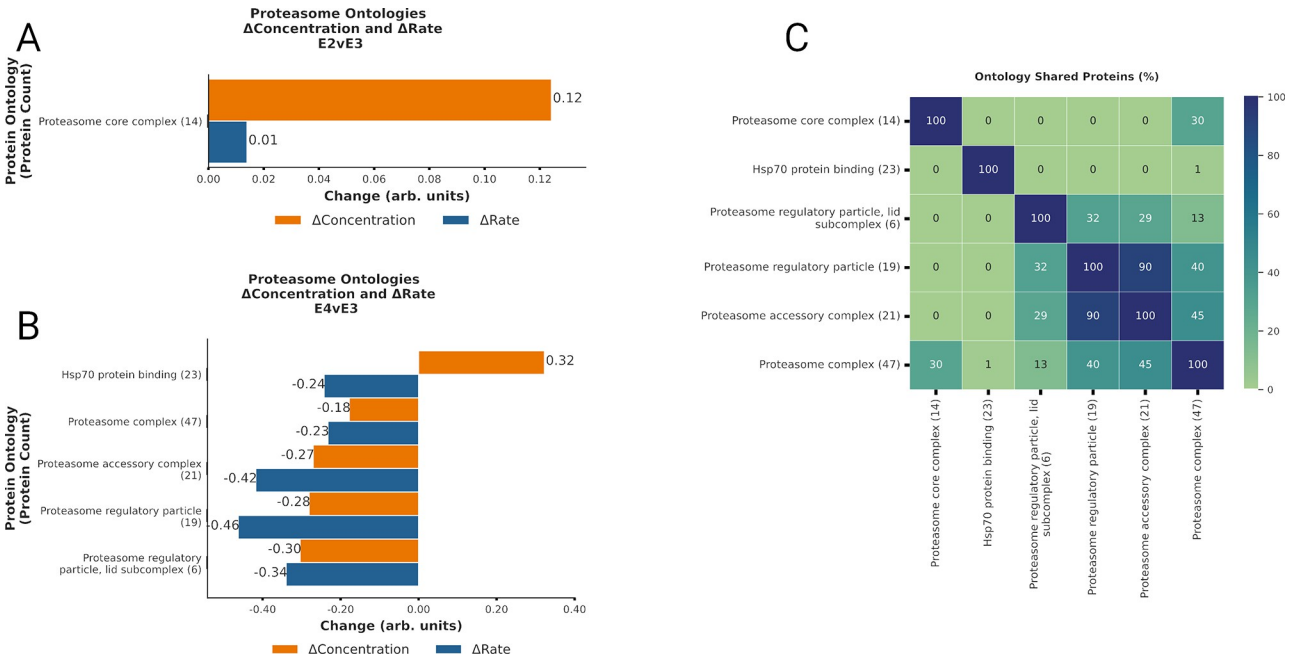

Fig 5. Proteasomal activity decreases with ApoE4 expression. A-B. Bar plot displaying Δabundance (orange) and Δturnover (blue) of proteins detected in all experimental cohorts for several ontologies related to proteasomal activity with significant* Δabundance in the E2vsE3 comparison (A) and in the E4vsE3 comparison (B). **C.** Heatmap displaying % of proteins shared across the ontologies with significant* Δabundance. ***(*BH-PV < 0.05)***. Created with Matplotlib.py and InkScape

https://doi.org/10.1371/journal.pcbi.1012407.g005

ApoE2 more efficient lysosomal processing will facilitate mitophagy based quality control while the inhibited lysosomal processing would inhibit mitophagy and make the ApoE4 more reliant upon individual protein replacement strategies.

ApoE4 Disrupts metabolic pathway control

We observed significant changes in Δabundance (BH-PV < 0.05) across multiple ontologies related to energy production (Fig 4). ApoE2 resulted in lower expression of levels of *Pyruvate metabolism (32)*, *Citrate cycle (TCA cycle) (26)*, and *Glycolysis/Gluconeogenesis (41)*. These reductions were primarily attributed to decreased synthesis (↓synthesis), a trend that was also evident in the *Oxidative stress and redox pathway (48)* proteins which protect the cell from reduced oxygen species. Notably, *Fatty acid beta-oxidation (25)* demonstrated reduced Δabundance coupled with increased Δturnover (↑degradation) in ApoE2 (E2vsE3), suggesting a potential decrease in fatty acid catabolism and an increase in the use of fatty acids for building complex lipids. In contrast, in the ApoE4 mice, major energy production pathways such as *Fructose and mannose metabolism (21)*, *Pyruvate metabolism (32)*, and *Glycogen metabolism (22)* all exhibited increased Δabundance and Δturnover, pointing towards enhanced synthesis of enzymes involved in carbohydrate metabolism in the E4vsE3 comparison and an increased reliance on carbohydrates for energy similar to previous observations [17,22].

ApoE Isoforms and Ubiquitin-Proteasome pathway activity

Proteasome-related ontologies exhibited significant changes in regulation due to ApoE isoforms (Fig 5). For both the E2vsE3 and E4vsE3 comparisons, we identified pronounced increases in Δabundance and reductions in Δturnover (↓degradation) associated with the *proteasome complex (47)* Furthermore, an increased Δabundance and Δturnover (↑synthesis) of

proteins involved in the *Regulation of ubiquitin-dependent protein catabolic process (62)* was statistically significant in both comparisons (BH-PV 0.05).

The *proteasome regulatory particle*, *base subcomplex (11)* displayed ↑synthesis in the E2vsE3 comparison and ↓degradation in the E4vsE3 comparison. Meanwhile, proteins within the *Proteasome regulatory particle*, *lid subcomplex (6)*, demonstrated significant Δabundance due to ↓degradation in the E4vsE3 comparison with ApoE4 expression. However, these changes were not significant in the E2vsE3 comparison. Additionally, in ApoE4 we noted ↑synthesis in the *Negative regulation of proteasomal ubiquitin-dependent protein catabolic process (21)*, ↓degradation *Deubiquitination (79)*, and ↓synthesis *Hsp70 protein binding (23)*. These observations suggest a nuanced regulation of the ubiquitin-proteasome system (UPS) in association with ApoE isoforms. Hsp70 proteins are often deemed pivotal regulators of proteasome activity [23]. These changes suggest a significant reduction in the proteasome-dependent protein quality control for ApoE4 tissue (Fig 5C).

Quantifying ApoE-dependent shifts in liver proteostasis

The liver is the largest producer of ApoE in the body and is also a major receptor of ApoE and its associated cargo [8,18,24]. Therefore, we tested whether the liver tissue from these same experimental mice would show matching ApoE allele-specific shifts in proteome regulation.

In contrast to the brain, ApoE2 liver there was no significant change in any of the endolysosomal processes relative to ApoE3 (S5 Table). Multiple mitochondrial ontologies in the liver changed in significant ways and nearly 60% of their proteostasis changes are equivalent to the brain. Most changes in the mitochondria in the liver with ApoE2 expression involve increased degradation of mitochondrial components, though there is some reduced synthesis for the mitochondrial envelope and transmembrane transport. Liver ApoE2 also did not shift proteasome-related ontologies in the same manner as the brain. In fact, where the brain contains decreased degradation of proteasomal components, the liver increases their synthesis and contains more proteasomal capacity similar to literature reports. [23,25,26]

In ApoE4/E3 liver comparisons there was not a significant change in any of the endocytic processes (S5 Table) with the exception of endosomal protein localization. Both tissues had increased concentration, through increased synthesis in the brain, while the liver decreased degradation. For ApoE4 mitochondrial components 80% of the significant mitochondrial liver ontologies had the same proteostasis changes in the brain (S5 Table). The 20% differences were due to certain NADH and ATP synthesis electron transport chain ontologies that were increased synthesis in the brain and increased degradation in the liver. Similar to the liver comparison of ApoE2 with the proteasome, in ApoE4 liver data there were no shared proteasome changes with the brain (Figs G and H in S1 File). These data suggest that most of the ApoE effects observed in the brain are not global.

Discussion

Exploring ApoE-genotype Effects Through the Lens of Proteostasis

Compared to the neutral ApoE3 allele, expression of ApoE4 significantly increases the risk for Alzheimers, while the expression of ApoE2 is moderately protective [5,8,12,22,25,27–29]. Here we investigate the etiology of these differences by measuring ApoE-dependent changes in protein homeostasis (proteostasis) in the tissues of human-ApoE transgenic mice (Fig 1A). Proteostasis is the dynamic control of concentration and quality [19,30–32] in the cell. According to our model (Figs 1C and B in S1 File), protein concentration is controlled by the competition between synthesis and degradation while protein turnover rate, or the rate that proteins are replaced, is the average of synthesis and degradation. We present this as simplified equations

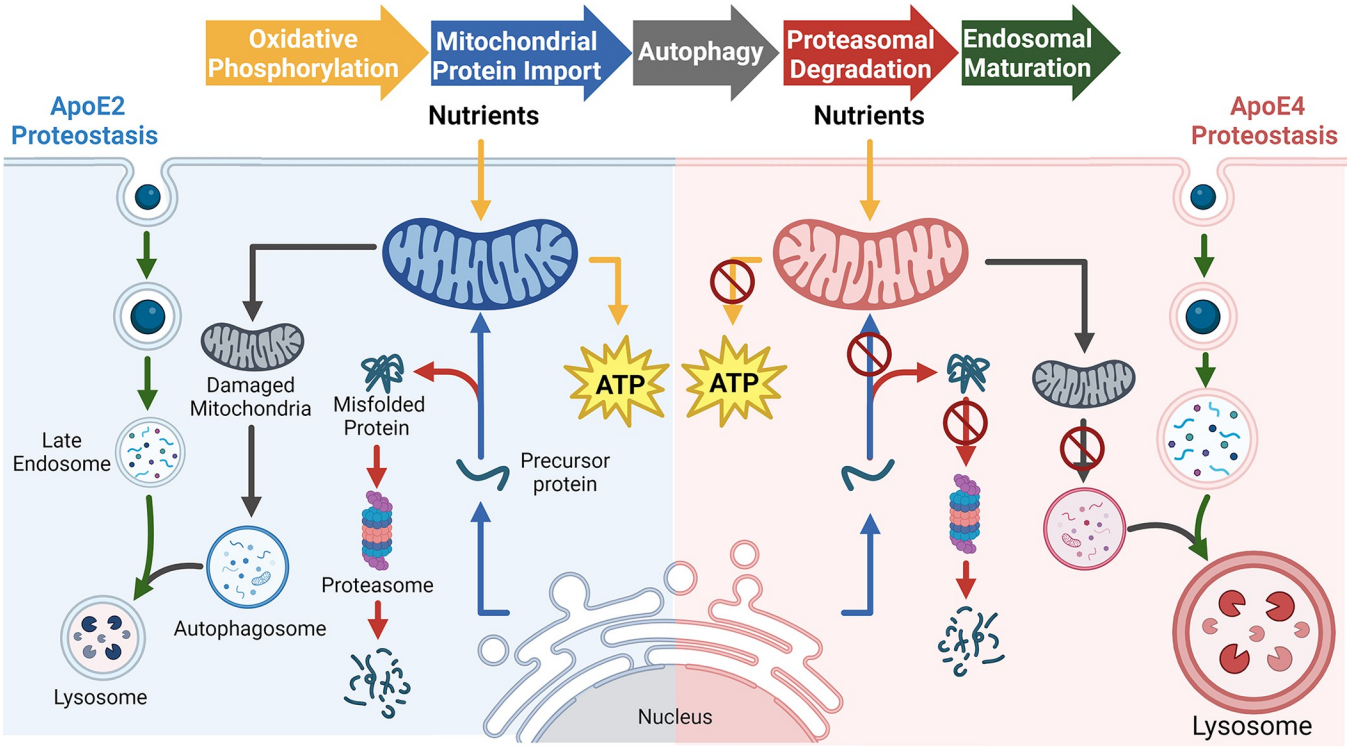

Fig 6. Model comparing the observed changes in proteostasis for ApoE2 and ApoE4. The arrows are color coded to represent the different pathways impacted in both ApoE2 and ApoE4 when compared to ApoE3. Created with Inkscape and Biorender.

https://doi.org/10.1371/journal.pcbi.1012407.g006

that relate to synthesis and degradation (see '*Proteostasis Model and Analysis Rational*' section for more detail). Therefore, changes in protein concentration (Δabundance, Eq 3) paired with changes in protein turnover rate (Δturnover, Eq 10) can highlight the regulatory balance of synthesis versus degradation between conditions (Fig 1B and 1C).

For instance, to increase abundance in the experimental condition (resulting in a positive Δabundance), cells can either synthesize faster or degrade slower. Alternatively, to decrease abundance (leading to a negative Δabundance), cells might reduce synthesis or increase degradation. Using the change in protein turnover rates (*Proteostasis Model* section, Eq 10) we can deduce whether changes in synthesis or degradation led to changes in abundance (Fig 1B). Therefore, a positive Δabundance indicates increased synthesis when Δturnover is positive or reduced degradation when Δturnover is negative. Conversely, a negative Δabundance signals increased degradation when Δturnover is positive or decreased synthesis when Δturnover is negative (Fig 1C). Applying this logic, we observed a cohesive pattern of ApoE-dependent changes in proteostasis regulation (Fig 6). Below, we discuss how our results unify a diverse set of literature observations for ApoE-dependent modifications of endosome trafficking, as well as lysosomal, mitochondrial, and proteasomal function.

ApoE isoforms modify Endocytic/Endosomal trafficking

Previous research has highlighted the dysregulation of endocytic pathways associated with ApoE4 expression [13,20,27,33–35]. We detected notable ApoE4-dependent changes in several ontologies related to endocytosis (Figs 2 and C in S1 File). This is in line with what is known about how ApoE isoforms modify affinity for cell surface receptors, such as LDLR and APOER2 [3,4], initiating the endocytosis of ApoE along with its content. After this endocytic

event, ApoE-laden endosomes undergo various maturation stages, wherein contents are earmarked for recycling, delivery, or degradation.

ApoE4 has a higher affinity binding to receptors [3,4] and induces a trafficking anomaly in the early endosome [33] leading to accumulation and enlargement of lysoendosomal compartments [13,20]. Following an endocytic event, the clathrin coat dismantles, allowing vesicles to fuse into various destinations for cargo release. This fusion mechanism leans heavily on SNARE and SNAP-receptor proteins, also pivotal for exocytosis. In our study, we observed diminished synthesis of SNARE and SNAP ontologies in ApoE4 mice which may disrupt vesicle fusion between organelles [36] and in response to exocytic sequences [37]. Our study revealed a reduced degradation of proteins associated with *Clathrin-mediated endocytosis (82)*, increased synthesis of *PICALM (90)*, and reduced synthesis of the *lysosomal membrane (70)* (Figs 2B and 2C in S1 File) in the presence of ApoE4. In the literature, ApoE4 expression induced a decline in clathrin-mediated endocytosis in astrocytes [38], dysregulation of early endosome populations in 18- and 25-month-old ApoE4 mice [34] and phosphatidylinositol binding proteins like PICALM [39]. Before undergoing lysosomal degradation, endosomes transition to the late endosomal phase. Our findings suggest that ApoE4 expression reduces the synthesis of both late endosomal and lysosomal membranes. Although the general *lysosome (146)* ontology exhibits increased degradation with ApoE4 expression, if we look specifically at the membrane components of this ontology then the ApoE4 specifically has less total protein due to lower synthesis. These results are consistent with previous observations of large-volume lysosomes which would have a low membrane surface/volume ratio accumulating in the in ApoE4 cells [13,20]. Collectively, these results underscore multiple points of failure in the ApoE4-associated inhibition of endosomal maturation and stalled lysosomal functions as previously observed [27,33,34].

The E2vsE3 tissue had similarities in vesicle-centric ontologies. Notably, there was a decline in the degradation of endocytosis and clathrin protein-related ontologies, and SNARE complexes saw reduced synthesis. This implies that ApoE2 also modifies vesicle endocytosis. However, the changes suggested a more streamlined regulation of endolysosomal events with ApoE2 (E2vsE3). This again agrees with literature reports of modified receptor binding with ApoE2 having lower affinity while ApoE4 has a higher affinity [3,4]. This coupled with lower degradation of proteins within the lysosome vesicle biogenesis ontology for the E2vsE3 comparison, a process intrinsically tied to endosomal trafficking and central to lysosomal adaptation [40], suggests a tighter control of endocytic events and better lysosomal quality with ApoE2 expression. These observations agree with previous research on astrocytes indicating ApoE2 expression increases lysosomal activity relative to ApoE3 and ApoE4 expression [41].

ApoE-dependent changes in Mitochondrial Proteostasis

We observed ApoE-dependent changes in mitochondrial proteostasis that were consistent with the modified autophagy and lysosomal function discussed above. In ApoE4 (E4vsE3) mice, we measured elevated degradation in *mitochondrial membrane (406)*, *mitochondrial inner membrane (303)* (Figs 3 and D in S1 File), *Cristae formation (11)*, *Mitochondrial fusion (13)*, and *mitochondrial transport (72)* with no accompanying change in *mitochondrial matrix (159)* and decreased synthesis of *mitophagy (18)*. Mitochondrial membrane complexes play critical functions in cellular homeostasis—such as energy production, calcium level modulation, apoptosis, and the regulation of reactive oxygen species (ROS) [42]. Prior research has documented dysfunction in the mitochondrial membrane's integrity as a promoter of Alzheimer's disease [43,44].

Most mitochondrial proteins are encoded on the nuclear DNA and are transported into the mitochondria through translocases (TIM and TOM) [45,46]. These translocases interact with

the many inner mitochondrial membrane (IMM) folds that make up the cristae via the mitochondrial cristae organizing system (MICOS).[47] Our observations indicate a change in mitochondrial protein import, especially evident in the higher degradation of the *TOM complex (10)*, *cristae formation (11)*, and the *MICOS complex* (7) ontologies. (See Figs 5B and 5E in S1 File). The MICOS also plays a vital role in cristae organization and the function of respiratory complexes.[48] Disruptions in MICOS have been documented to modify cristae structure[49], and recent studies associate altered MICOS protein expressions with ApoE4 manifestation [44]. The MICOS literature also report evidence of mitochondrial fusion and fission imbalance in Neuro-2a cells expressing ApoE4.[44] Previous analysis of AD brains indicated diminished protein levels connected to mitochondrial fusion/fission[50], which our data supports as a degradation driven loss of fusion proteins (See Figs DA and DB in S1 File).

Mitochondria and the endoplasmic reticulum (ER) collectively form the mitochondria-associated membrane (MAM), which has implications in AD pathology [51,52]. These MAMs regulate oxidative phosphorylation, calcium levels, protein degradation, and mitochondrial membrane organization. Our dataset elucidates an ApoE4-induced *MAM (57)*, marked by increased degradation contrasted against ApoE3 (Figs 3 and D in S1 File). Our results support ApoE4-related MAM instability by diminished synthesis of chaperone complexes, mitophagy, and calcium transport.

These results suggest that ApoE4-tissue relied on replacement of individual components within the mitochondria to maintain homeostasis. In contrast, ApoE2 mice increased degradation of mitochondrial membrane ontologies with a matching increase in the degradation of the matrix proteins. Although both ApoE2 and ApoE4 mice revealed changes in the mitochondrial membrane and transport, our ApoE2 findings suggests that there is a cohesive organelle-wide response involving both membrane and matrix proteins. Combined with the endolysosomal systems results, we postulate this might be evidence of superior mitophagy in ApoE2. Additionally, we theorize, as described in the literature [17,21,22,44,53], that the disparate attempts at protein replacement in ApoE4 mitochondria culminate in dysfunction.

ApoE disrupts ATP production

There is an increasing body of research on ApoE genotype-specific effects in ATP production [54–56] which links compromised bioenergetic pathways to neurodegeneration [57–60]. Several studies highlight an ApoE4-related shift towards glycolysis and diminished oxygen consumption in brain tissues. [22,57,61] Our data align with these observations, with increased synthesis of carbohydrate metabolism ontologies in ApoE4 (see Fig E in S1 File). These ontologies include *Fructose and mannose metabolism (21)*, *Pyruvate metabolism (32)*, and *Glycogen metabolism (22)*. We posit that this increased reliance on carbohydrate metabolism is a consequence of the lack of cohesive mitochondrial maintenance.

While ApoE4 expression is associated with diminished ATP production [54,62–64], ApoE2 expression has been shown to enhance ATP production and glycolytic activity [57,61]. In ApoE2 tissue, we observed decreased abundance in ontologies such as the *TCA cycle (25)*, *Pyruvate metabolism (32)*, and *Glycolysis / Gluconeogenesis (41)* due to diminished synthesis and augmented degradation. These regulatory changes are different than expected based on the literature. This might be because our study averages together all cell types and regions of the brain and therefore may diverge from cell type-specific experiments. Collectively, our data accentuates the isoform-specific alterations in diverse metabolic pathways and suggests that isolating single cell types or regions from the brain may be important to test for metabolic changes in response to ApoE isoforms.

Linkages between the Proteasomal and Mitochondrial Homeostasis

The proteasome also plays a major role in the mitochondrial quality control, by degrading excess or misfolded proteins that disrupt mitochondrial activity [65], and saving cells from misfolding stress response. [66] Reduced proteasome activity has consistently been implicated as a major player in the pathophysiology of neurodegeneration [21,25,26,67,68]. ApoE2 has been shown to directly inhibit the cleavage of amyloid precursor protein (APP) to decrease Aβ peptide formation. [69]while ApoE4 may promote its accumulation. [10,13,70–72] This buildup of Aβ has been shown to directly inhibit proteasome function leading to increased accumulation of amyloid plaques. [73,74]

Proteasome function can also be disrupted by mitochondrial dysfunction. For example, oxidation of the 26S subunit of the proteasome due to increased mitochondrial oxidative stress has been shown to increase the accumulation of ubiquitinated substrates and decrease proteasomal activity [75]. Notably, we discerned a significant reduction in the synthesis of HSP70 proteins in E4 which latch onto misfolded or compromised proteins before proteasomal degradation [23]. This interconnection of the proteasome and mitochondria as well as their consistent implication in neurodegenerative disease has led some researchers to suggest that dysfunction in either the proteasome or mitochondria are "two sides of the same coin" leading to a futile cycle of mitochondrial and proteasomal insult. [76]

ApoE2 also reduced the degradation of the proteasome, paralleling the ApoE4 response (see Figs 5 and F in S1 File). While both ApoE2 and ApoE4 increase synthesis of 'ubiquitin-dependent catabolism' ontologies, the regulatory complex of the proteasome (responsible for facilitating the unfolding and admission of ubiquitinated polypeptides into the proteasome's degradation chamber [77]) the 'negative regulation of catabolism' had increased synthesis in ApoE4. This implies larger proteasome pool in ApoE4, albeit with more regulation.

Our data on proteasomal and lysosomal regulation in ApoE4 are in agreement with existing literature [33,78], suggesting that suboptimal endocytic regulation might directly impact autophagy and the proteasomal maintenance of mitochondrial proteostasis. Our findings also substantiate the ApoE4-associated dysregulation of MAM structures [22,51,52], which potentially results in disrupted mitochondrial morphology and impaired energy production. Our working hypothesis postulates that ApoE4 expression reduces autophagy and proteasomal activity, diminishing capacity to eliminate dysfunctional mitochondria.

Liver Proteostasis Changes Compared to Brain

ApoE is an important lipid transporter to many parts of the body, not just the brain. Although ApoE2 protects against Alzheimer's Disease, it increases risk for cardiovascular disease [18]. This leads us to question if the mechanism by which ApoE2 protects against Alzheimer's, may be detrimental and disease causing to other tissues. To understand if ApoE elicits a global response across all tissue, we tested and analyzed the liver tissue from our experimental mice in the same manner as the brain.

The changes in ApoE2/E3 liver and brain proteostasis were not equivalent. Although many trends were similar between brain and liver, few changes in the liver were statistically significant. Mitochondrial protein localization, transportation, and organization had similar proteostasis trends between tissues, that suggest mitochondrial turnover to be reduced in the liver compared to the brain (S3 Table compared to S5 Table).

Similarly, ApoE4/E3 liver and ApoE4/E3 brain proteostasis changes in the endosome, metabolism, and proteasome pathways in the brain are not similar between tissues (see S4 and S5 Tables). However, significant effects of ApoE4 regarding the mitochondria between the

liver and brain contained several of the same proteostasis changes, suggesting there may be some degree of shared effects due to ApoE4.

Thus, while some cellular pathways may be affected similarly, a global effect specific to ApoE allele is not observed in our data. We propose the lack of a global ApoE effect (Figs G and H in S1 File) is because most tissues have a large number of apolipoproteins (~16) participating in lipid transport [8,18]. The brain is limited to the apolipoproteins that it creates (primarily ApoE and ApoJ), and ApoA1 which can cross the blood-brain-barrier [16]. Since lipid trafficking in the liver involves many more apoliproproteins, this may dilute the ApoE effect. Future experiments investigating peripheral tissues that only receive ApoE from the liver could help distinguish if the ApoE-dependent changes in the brain are due to endocytosis and internalization of the ApoE-specific cargo.

Conclusion

In this study, we demonstrated how combining protein abundance and turnover rate unveils the cellular regulation of protein synthesis and degradation. Utilizing proteomics data, we compared ontology-level variations due to ApoE genotypes in healthy adult mice. Our findings present *in vivo* evidence that harmonizes with existing literature, linking brain ApoE4-dependent changes in endosomal trafficking, autophagy, proteasome activity, and lower mitochondrial quality. Concurrently, our data suggests that ApoE2 enhances brain mitochondrial health by increasing turnover in tandem with a corresponding increase in proteolysis capacity in the brain (Fig 6). Future work investigating ApoE-dependent modification of region-specific lipid transport or protein-protein interactions will be necessary to elucidate the key initiating variables causing these proteostatic changes.

Methods

Ethics statement

All animal handling experiments were reviewed and authorized by the Brigham Young University Institutional Animal Care and Use Committee (IACUC protocol #191102).

Experimental design and statistical rationale

Cohort Grouping and analysis rationale. A total of 72 homozygous ApoE transgenic mice, with an equal distribution of female and male individuals were included (Fig A in S1 File). This cohort included 24 ApoE2, 24 ApoE3, and 24 ApoE4 (refer to S1 Table for details). The sample groups for protein turnover rate measurements of each ApoE genotype and gender, were two independent blocks of six mice. [79] These six mice were selected based on the metabolic labeling duration, namely Day 0, Hour 6, Day 1, Day 4, Day 16, and Day 32 post-exposure to deuterium.

The kinetic analysis utilized peptide identifications from LC-MS/MS acquisition files to extract isotope envelope information from LC-MS (MS1 only) data. Notably, this process heavily relies on peptide retention time. To facilitate this, MS/MS data and MS data were collected within the same randomized block of samples. [79] The initial four timepoints (Day 0, Hour 6, Day 1, and Day 4) were used to generate LC-MS/MS fragmentation spectra and identify peptide sequences with observed charge and retention time.

To streamline sample processing and turnover rate measurements, mice were organized into four gender-specific groups of 18 mice (n = 6 per genotype, Fig A in S1 File). This grouping strategy accommodated instrument availability and minimized retention time deviations associated with extensive sample worklists. [79] Additionally, from each group, a subset of

four mice per genotype, comprising the first four timepoints (Day 0, Hour 6, Day 1, Day 4), were selected for LFQ proteomics. This selection yielded a total of 16 mice per ApoE genotype for an area under the LC curve (Abundance) fold change (FC) calculations, with an equal distribution of 8 females and 8 males in the four gender-specific groups. Thus, out of the initial 72 mice, 48 were used to generate the "Abundance" FC values (Fig A in S1 File).

To broaden proteome coverage, each brain homogenate sample was fractionated into cytosolic and membrane components, which were prepared and analyzed separately using the workflow described below. This fractionation led to the creation of eight datasets for our analysis. Each dataset underwent individual processing using the Peaks Studio software (Bioinformics Solutions Inc.) for protein abundance and Deuterater software for turnover rate measurements. Protein-level abundance fold change relative to control (FC values), turnover rate FC values, and statistical analysis (P-value) for each comparison (e.g., E2vsE3) were calculated for each dataset independently to minimize inter-set variance caused by sample prep discrepancies, instrument noise, buffer compositions, and sample run variables. Due to problems in sample processing, the Hour 6 sample was omitted from a single ApoE4 dataset (D16 was substituted for LFQ analysis), and Day 4 was omitted from a single ApoE3 LFQ dataset (S1 Table).

While FC and P-value calculations for abundance and turnover were conducted at the protein level, this study mainly focuses on how proteins with shared functional characteristics are regulated in an ApoE isoform-specific manner. To achieve this, the StringDB multiprotein tool [80] was employed to identify functional groups (ontologies) represented in the final data sets (Abundance FC, Turnover FC). Every protein Abundance FC value was calculated with a minimum of three biological abundance measurements in experimental (ApoE2, or ApoE4) and control (ApoE3); see the 'Protein ΔAbundance Analysis' section for more details. The null hypothesis (H0) posited that proteins' collective gene expression ratio in an ontology would remain unchanged (H0: Abundance FC = 1) across ApoE genotypes. Consequently, we tested the alternative hypothesis that ApoE genotype alters the regulation of functionally related protein groups (Ha: Abundance FC $\neq$ 1) using a one-sample t-test. This analytical approach captured changes occurring across the broader functional proteome rather than focusing solely on identifying individually significant proteins. Python code created for both protein- and ontology-level calculations is available in the GitHub repository JC-Price/PublicProteomeDataAnalysis: scripts for proteome data wrangling.

Proteostasis model and analysis rational. A protein homeostasis model must account for common sources and sinks of protein mass (Fig B in S1 File). In this model, we assume there is a large circulating pool of free amino acids affected by diet, metabolites, and waste expulsion. Amino acids become the precursors for protein synthesis in an initial tRNA charging step, which then polymerize in an mRNA-dependent step before folding into functional proteins. Multiple competing processes subsequently influence the resulting protein concentration. First, degradation returns the protein to the constituent amino acids in the free pool. The functional proteins may also transition (reversibly) into an aggregate/condensate state that undergoes a separate degradation process. Finally, protein concentration may be affected by importing or exporting proteins.

Our goal is to use chemical kinetics and translate this diagram into a mathematical model with a few tunable parameters identifiable from experimental data. Unfortunately, a complete mathematical translation of this system leads to a model with too many parameters to draw meaningful conclusions. We, therefore, make several simplifying assumptions about which processes are dominant to restrict the parameters to an identifiable subset.

First, the mice in this study are healthy adults, so we assume the protein concentrations are in steady-state with no protein aggregate. We assume that the pool of free amino acids is large

so that the rate bottleneck in the tRNA-charging/synthesis/folding steps is synthesis and that import/export is negligible. We also assume the protein pool is well mixed, assuring the random selection of protein for degradation (unregulated). Although reasonable for the present study, these assumptions are bad for surprisingly large sections of the proteome where reversible aggregation [81,82], multistage regulation of synthesis rates [83–85], regulated exchange of protein subunits in complexes [86, 87] and nonrandom degradation [32,67,88,89] are biologically important, but we maintain them as a starting point for the modeling. Previous literature reports have presented mathematical modeling of protein turnover rates using similar assumptions. [31,90–96] This then results in Eq 1 where the time-dependent change in a protein concentration is the difference between the synthesis and degradation rates.

$$\frac{dP}{dt} = k_{syn} - k_{deg}[P] \tag{1}$$

This model assumes that the concentration of an individual protein ([P]) in every location is under the control of a zero-order synthesis rate (k_{syn}) and a concentration-dependent degradation (k_{deg}) step. The assumption of zero-order synthesis suggests that the precursor is stable and unresponsive to protein concentration, while a first-order rate for degradation suggests that there is no regulation of degradation other than protein concentration. In general, the rates k_{syn} and k_{deg} need not be constant as they are under the control of numerous exogenous factors that may vary in time. However, we now formalize our final assumption: protein homeostasis. This assumption is that the multiple processes regulating each protein concentration are in dynamic equilibrium so that these rates are constant for a given experimental condition. Synthesis and degradation for a given protein are equal, ensuring that the number of proteins produced is equal to the number of proteins lost. [19] Therefore, during the measurements d[P]/dt = 0, leading to the relationship:

$$[P] = \frac{k_{syn}}{k_{deg}} \tag{2}$$

Our hypothesis is that the expression of the ApoE polymorphisms (ApoEx = ApoE2 or ApoE4) creates a unique steady state or proteostasis across the proteome that can differ from the concentration of the human wild-type control (ApoE3). The change in protein abundance (Eq 3) between the two conditions allows us to infer how the ratio of the rates is changed in the experimental cohorts, but neither k_{syn} nor k_{deg} is individually identifiable.

$$\Delta Abundance = \frac{d[P]}{dApoE} = \left(\frac{k_{syn}}{k_{deg}}\right)_{ApoEx} - \left(\frac{k_{syn}}{k_{deg}}\right)_{ApoE3} \tag{3}$$

Using metabolic isotope labeling we can add rate information that will distinguish between changes in synthesis and degradation. Assume that at t = 0 our model simplifications are true, but that the amino acid pool is replaced with a deuterated version. Proteins synthesized after t = 0 are isotopically labeled, and we can measure the time-dependent replacement of old unlabeled for new labeled proteins. To make this mathematically explicit, we denote the concentration of normal proteins by [P] and the concentration of deuterated proteins by [P^D]. These two concentrations now satisfy the initial value problems.

$$\frac{d[P]}{dt} = -k_{deg}[P], [P](0) = \frac{k_{syn}}{k_{deg}} \tag{4}$$

and

$$\frac{d[P^D]}{dt} = k_{syn} - k_{deg}[P^D], [P^D](0) = 0 \quad (5)$$

These are true because normal proteins are no longer being synthesized (Eq 4) and [P^D] have no initial concentration (Eq 5). These ordinary differential equations can be solved in closed-form using standard techniques. The solutions are:

$$[P]_t = \frac{k_{syn}}{k_{deg}}\left(e^{(-k_{deg}t)}\right) \quad (6)$$

and

$$[P^D]_t = \frac{k_{syn}}{k_{deg}}\left(1 - e^{(-k_{deg}t)}\right) \quad (7)$$

Notice that these equations satisfy $[P]_t + [P^D]_t = k_{syn}/k_{deg}$, which is independent of time as it must be in homeostasis. However, the measurable fraction of deuterated protein over time is given by.

$$\frac{[\boldsymbol{P^D}]}{[\boldsymbol{P}] + [\boldsymbol{P^D}]} = \mathbf{1} - \boldsymbol{e}^{-\boldsymbol{k_{deg}t}}, \quad (8)$$

Eq 8 seems to suggest that the degradation rate is the measurable driving force behind the turnover of old protein and the replacement by labeled protein. However, because the processes of synthesis and degradation are exactly balanced in the proteostasis condition, we can just as easily identify the turnover rate as the per-molar synthesis rate: $k_{syn}/[P]$ or fractional synthesis [97] as it is commonly called. It is important to emphasize that these rates are only properly defined in homeostasis. Because there is no assurance that homeostasis is equally applied to all proteins simultaneously[85, 88, 98], we find it conceptually preferable to define the turnover rate as the mean of the per-molar synthesis and degradation rates:

$$k_{turnover} = \frac{1}{2}\left(k_{syn}/[P] + k_{deg}\right) \quad (9)$$

As stated above each experimental mouse cohort will have a unique homeostasis with a protein-specific synthesis and degradation rate. Using ApoE3 as our normal control we can assess how the average of the synthesis and degradation rates have changed with the E2 and E4 polymorphisms (ApoEx).

$$\Delta Turnover = \frac{1}{2}\left(\left(\frac{k_{syn}(ApoE_x)}{[P](ApoE_x)} - \frac{k_{syn}(ApoE_3)}{[P](ApoE_3)}\right) + \left(k_{deg}(ApoE_x) - k_{deg}(ApoE_3)\right)\right) \quad (10)$$

This means that if, for example, the ApoE polymorphism increases a protein concentration (+*ΔAbundance*, Eq 3) the *ΔTurnover* (Eq 10) will highlight whether the change in proteostasis was driven by an increase in $k_{syn}/[P](ApoEx)$ or a decrease in $k_{deg}(ApoEx)$ because the sign of *ΔTurnover* will be different for each possibility. Together the experimental *ΔAbundance* and *ΔTurnover* for each protein identifies whether the differences in proteostasis are primarily due to changes in synthesis or degradation. Graphing these values produces a plot where each quadrant (Fig 1C) has meaning. For example, a positive x-axis (+Δabundance) and y-axis (+Δturnover) suggest that synthesis increases (Syn↑). Conversely, a protein with lower expression levels (-Δabundance) between ApoE genotypes, could result from less synthesis (Syn↓) if

turnover rate decreases (-Δturnover) or more degradation (Deg↑) if the protein turnover rate increases (+Δturnover). Since, each measurement has independent noise, a nonrandom enrichment of multiple proteins from a functionally related ontology within a quadrant is an important metric of confidence that the cell is regulating protein expression to change biochemical functions (Fig 1D and 1E).

Mouse handling

The mouse model employed for this study consists of ApoE knockout C57BL/6 transgenic mice that express one of the three human ApoE alleles (ApoE2, ApoE3, ApoE4, n = 24/allele, see S1 Table) homozygously under the GFAP promoter (JAX# 004632, 004633, 004631). Notably, this model has provided valuable insight into genotype-specific effects of ApoE in a large number of other experiments [70,71,99–108]. This study does not encompass differences from wild-type mice. The transgenic mice were selected with deliberate focus on ApoE isoforms rather than wild-type conditions, or age differences. The findings reported in this publication use fold change relative to ApoE3 to minimize the GFAP promoter variable as reported previously [10,11,109]. Because mouse ApoE has a low sequence identity (77%) and a different transcription promoter, the human ApoE3 model is the best control for comparison. While we recognize the limits of a transgenic model, this study provides valuable identification of *in vivo* patterns which can be confirmed in future ApoE knock-in mice models and human studies. These results refer solely to the effects of ApoE isoform differences, rather than Alzheimer's Disease. Similarly, these results represent the weighted average across the entire mouse brain. We presume that some brain regions will have differential sensitivity. [14,22,34] Any claims regarding Alzheimer's disease are made solely to highlight similarities between current ApoE/AD research and our observations to create a holistic mechanistic hypothesis.

Mice were randomly selected for replicate designation and timepoint based on availability. They were all 6–8-month-old, retired breeders with no signs of disease or neurological dysfunction. There were no exclusions among this group. Specific cohort denominations and animal numbers can be found in Fig A in S1 File. Blinding was not used during any portion of this experiment as it was necessary to compare groups at each point. Mice were housed together in the same room of the facility at the same time. Mice had *ad libitum* access to water and standard nutritional rodent feed (Teklad 8604) while housed in a temperature-controlled environment of ~24˚C. This environment included a 12-hr circadian cycle. To initiate turnover rate measurements, mice received an intraperitoneal (IP) injection of sterile D_2O 0.9% w/v saline (35 μl/g body weight) calculated to increase internal D_2O concentrations to an initial 5% of overall water weight (w/w). Mice were then given 8% D_2O as the sole hydration source for the remainder of the experiment. This was done to maintain overall internal water at 5% D_2O enrichment. Mice were sacrificed according to the following timepoints post IP injection: day 0 (no D_2O injection), hour 6, day 1, day 4, day 16, and day 32. Mice were euthanized via CO_2 asphyxiation followed by bilateral thoracotomy. Blood was collected via cardiac puncture for D_2O enrichment calculations. Brains were divided sagittally into respective hemispheres. Brain and liver were flash frozen on blocks of solid CO_2. Tissues were stored frozen at -80˚C until processing.

Tissue preparation

Singular brain hemispheres and liver sections were homogenized in lysis buffer (25mM Ammonium Bicarbonate treated with diethylpyrocarbonate and ThermoScientific Halt Protease & Phosphatase Inhibitor Cocktail) for 60 sec using a MP FastPrep-24 homogenizer. Homogenized samples were centrifuged for 15 minutes at 14,000xg to separate them into

cytosolic and membrane isolates. The membrane pellet was resuspended in lysis buffer and centrifuged for 15 minutes at 14,000xg a total of three times to remove cytosolic components. Each fraction was resuspended in 5% SDS. Aliquot concentration was measured via a Pierce BCA Protein Assay Kit purchased from ThermoFisher Scientific, and 50 μg of protein were prepared according to S-Trap documentation (cytosol and membrane fractions were prepared separately). Proteins were digested with trypsin Lys/C overnight at 36˚C. Resultant peptides were dehydrated in a ThermoScientific Savant SPD131DDA SpeedVac Concentrator and resuspended at a final concentration of 1 μg/μL in buffer A (3% acetonitrile, 0.1% formic acid).

LC-MS

Samples were separated and measured via liquid chromatography-mass spectrometry (LC-MS) on an Ultimate 3000 RSLC in connection with a Thermo Easy-spray source and an Orbitrap Fusion Lumos. Peptides were pre-concentrated with buffer A (3% acetonitrile, 0.1% formic acid) onto a PepMap Neo Trap Cartridge (particle size 5 μm, inner diameter 300 μm, length 5 mm) and separated with an EASY-Spray HPLC Column (particle size 2 μm, inner diameter 75 μm, length 25 mm) with increasing buffer B (80% acetonitrile, 0.1% formic acid) gradient:

0–5 min, 0 to 5% B; 5–87 min, 5 to 22% B; 87–102 min, 22 to 32% B; 102–112 min, 32 to 95% B; 112–122 min, 95% B; 122–125 min, 95 to 2% B; 125 to 127 min, 2% B; 127–129 min, 2 to 100% B; 129–132 min, 100% B; 132–133 min, 100 to 2% B; 133–135 min, 2% B; 135–137 min, 2 to 100% B; 137–140 min, 100% B; 140–142 min, 100 to 0% B; 142–144 min, 0% B.

The MS-based data-dependent acquisition method was set to a 3 second cycle time. MS1 scans were acquired by the Orbitrap at a resolution of 120,000. Precursors with a charge > 1 and < 6 were selected for MS2 fragmentation. MS2 scans of CID precursor fragments were detected with the linear ion trap at a scan rate of 33.333 Da/sec with a dynamic injection time. CID collisions were set to 30% for 10ms. A 60 second dynamic exclusion window was enabled; isotopes and unassigned charge states were excluded. The deuterium labeling information was collected separately in an MS1-only acquisition with the Orbitrap at a resolution of 60,000 as previously described by Naylor et al. [110]

Raw Data Processing for Peptide Identification and Label-free Quantitation

Raw files were searched against the 2022 Uniprot/Swissprot *mus musculus* FASTA (containing 17144 entries) using Peaks Studio v.11 (Bioinformics Solutions Inc.) for label-free quantitation (LFQ) analysis. During the data refinement step, the feature "associate feature with chimera [DDA]" was selected to deconvolute scans with co-eluted isobaric peptides. The parent mass error tolerance was set to ±15 ppm and the fragment mass error tolerance was set to 0.5 Da. Cysteine carbamidomethylation was set as a fixed modification, and both methionine oxidation and pyro-glu from glutamine were set as variable modifications in the search. Digest mode was set to semi-specific for the trypsin-lysC enzyme mix allowing for ≤ 3 missed cleavages and the peptide length range was set to 6–45 amino acids. The false discovery rate (FDR) for peptide matches was set to 1%, and protein ID significance was set to -10log(P-value) ≥ 15 for each identified protein.

Peaks Studio (Bioinformics Solutions Inc.) was also used to search raw files for use in Deuterater [110] software. The raw files were searched against the 2021 Uniprot/Swissprot *mus musculus* FASTA (containing 17144 entries). Peptide searches were performed using trypsin/lysC semi-specific digest with a tolerance of ±20ppm and missed cleavages ≤ 3. Carbamidomethylation was set as a fixed modification and pyro-glu from glutamine and methionine

oxidation were set as variable modifications. Within the Peaks Studio DB module, proteins were identified with two or more unique peptides at an FDR of 2% and significance was set to -10log(P-value) $\geq$ 15 for each identified protein.

Protein ΔAbundance analysis

The group of mice used in this paper were divided into two male and two female groups for analysis [79]. Each group produced a dataset for cytosolic proteins and another dataset for membrane proteins. Please refer to the *Experimental Design and Statistical Rationale* section for more information resulting in a total of eight datasets.

Data filtering, normalization, and quantitative calculations were performed independently for each dataset following standardized metrics for data quality and analysis following the process described by Aguilan et al. [111] Each Peaks Studio DB *protein.csv* output dataset contains the proteins identified in the analysis and the expression values (relative abundance) for each protein in each sample are labeled as "Area". This output was filtered to retain only the top proteins in each protein group and proteins with at most one missing protein "Area" value per genotype (i.e., n– 1/genotype/dataset). Subsequently, protein "Area" values in the dataset underwent $\log_2$ transformation. The distribution of these protein "Area" values was mean centered by subtracting by the average protein "Area" from each protein "Area" within the sample. To ensure comparability across samples, the distribution width was also normalized between samples by calculating the correlation slope between these total average protein "Area" values across all samples and the individual sample values. Each protein "Area" in a sample was then divided by the corresponding sample slope. For samples with a missing protein "Area" value, imputation was carried out using the scikit-learn KNN imputer function module in python with the two closest neighbors. [112]

Protein fold change (FC) values, which represent the relative change in protein abundance values ("Area") compared to a reference, were calculated, and used as a metric of change in abundance (Δabundance). For this study, FCs were calculated for protein expression values in ApoE2 mice and ApoE4 mice with ApoE3 expression values as reference, respectively. As per Aguilan et al.'s methodology, an F-test was employed to assess the variance between protein expression values before performing p-value calculations for statistical significance. To evaluate the statistical significance of expression levels in each comparison, a two-sample independent t-test (homoscedastic) was employed for proteins with an insignificant F-test result and a two-sample independent t-test (heteroscedastic) for proteins with a significant F-test result. Both the F-test and t-test calculations were conducted with the Scipy python package. [113]

Protein FC values were averaged across all datasets for each respective comparison. This produced a single set of "Area" (expression value) FCs for each comparison. Please note that both the ApoE2 vs ApoE3 (E2vsE3) comparison and the ApoE4 vs ApoE3 (E4vsE3) use the same list of quantified proteins. As outlined by Van den Berg [114], protein FC values from individual comparisons were range scaled using the following formula prior to ontology exploration:

$$x\prime_{ij} = \frac{x_{ij} - \bar{x_i}}{x_{i_{max}} - x_{i_{min}}} \tag{11}$$

Where x'_{ij}, x_{ij}, $\bar{x_i}$, x_{imax}, and x_{imin} are the scaled FC value, non-scaled FC value, mean FC, largest FC, and smallest FC, respectively. Range scaling was selected because it captures relative change in protein expression while considering the full range of values specific to the dataset. These scaled FC values will be utilized in functional analyses as described in the *Ontology-level Calculations* section below. The python script created for the steps outlined in this quantitative

analysis can be found in the GitHub repository JC-Price/PublicProteomeDataAnalysis: scripts for proteome data wrangling.

Protein ΔTurnover rate calculation

Protein turnover rate values were calculated using Deuterater[110] v5. This software uses an accurate mass and time database to extract peptide isotope patterns from LC-MS (MS1) centroided data utilizing feature identifications (e.g. retention time, mass, peptide ID, etc.) obtained from MS/MS data (refer to the *Raw Data Processing for Peptide Identification and Label-free Quantitation* section above).

Isotope patterns were extracted from MS1 raw data with an extraction retention time window of 1.5 min and an m/z error limit of $\leq$ 30 ppm. The n-value represents the number of available positions on a peptide where deuterium can replace hydrogen. In the *theory generation* step, peptides with data missing in an extracted file are removed, and the n-value is calculated for remaining extracted peptides based on known quantities for each amino acid [115,116]. Subsequently, *Fraction New* measures the amount of turnover rate for each peptide in a file by calculating changes in neutromer abundance and spacing [110]. These calculations were performed using the average between M0 and the highest isotope peak for peptides meeting specified criteria, including peptide n-values greater than 5, a minimum peptide sequence length of 6, and a minimum allowed M0 change of 0.04. In the *Rate Calculation* stage, the data from the *Fraction New* step is fitted to a kinetic rate curve using **Eq** 8 from our proteostasis model. Turnover rates were calculated for peptides that met a specified criterion, including a minimum of 3 non-zero peptide timepoints, and measurement deviation of less than 0.1, as previously reported [86]. The asymptote value is assumed to be 1 in the first iteration of analysis for proteins, but not for lipids where multiple pools of the same lipid are frequently observed [117].

After the Deuterater [110] analysis, all proteins with a valid turnover rate value (Rsq $\geq$ 0.6, combined unique peptides $>$ 1, combined rate $>$ 0) grouped by allele cohort, and the average turnover rate value was calculated for each protein in the cohort, respectively. These protein turnover rate values were $\log_2$ transformed, and the protein turnover rate FC was calculated as the difference of the $\log_2$ rates. The ApoE2 mice and ApoE4 mice were compared to the reference ApoE3 mice, resulting in a single set of protein turnover rate FCs for each comparison. To standardize the protein turnover rate FCs, auto scaling [114] was applied, where x'_{ij}, x_{ij}, $\bar{x}_i$, and s_i are the scaled turnover rate FC value, non-scaled turnover FC value, mean turnover FC rate and turnover rate FC standard deviation, respectively:

$$x\prime_{ij} = \frac{x_{ij} - \bar{x}_i}{s_i} \tag{12}$$

Auto scaling was implemented because it considers both the mean and standard deviation to reduce the effects of outliers and variation in the data while preserving the ability to focus on small changes. It is important to note that because of the signal to noise requirements fewer proteins had valid turnover rate FC values than quantifiable abundances. Consequently, proteins with turnover rate FCs represent a smaller subset population in comparison proteins with expression value FCs calculated from "Area" values. These protein turnover rate values were used for ontology analysis as outlined in the *Ontology-level Calculations* section below. For further reference, the python script created to process the *calculated_rates* output from Deuterater [110] can be found in the GitHub repository JC-Price/PublicProteomeDataAnalysis: scripts for proteome data wrangling

Ontology-level calculations

The StringDB [80] multiprotein tool was employed to calculate group FC values for functionally-related protein groups (ontologies) regardless of statistical significance. To streamline the analysis and reduce the number of redundant term ID (ontologies), ontologies were selected only from the following established: *GO Process*, *GO Function*, *GO Component*, *KEGG*, *Reactome*, and *WikiPathways*. To quantify the representation of each ontology, the "observed gene count" was divided by the "background gene count" to calculate the "Ontology_coverage (%)" for each ontology. Only ontologies with $\geq$25% were included in this analysis. This latter criterion ensures that the identified ontologies are sufficiently represented in the data (S4 and S5 Tables).

The "matching proteins in your network (labels)" was used to associate each observed protein in the ontology with the calculated "Area" FC and turnover rate FC, respectively, for both the E2vsE3 and the E4vsE3 comparison. Next, the average protein "Area" FC and turnover rate FC was calculated for each identified ontology by averaging the FC values of proteins within that category. This step summarized the collective expression and turnover rate changes of proteins within specific functional groups for each comparison.

To assess the statistical significance of the FC values within each ontology, a one-sample t-test with null hypothesis (H0) stating the average ΔAbundance (**Eq** 3) for the ontology is equal to 0, and the alterative hypothesis (Ha) indicating that it is not equal to 0. This statistical test is used to determine whether the observed changes in protein expression for the ontology, as a whole, were statistically significant. To account for multiple comparisons and maintain a controlled false discovery rate (FDR), the Benjamini-Hochberg correction (BH-PV) was calculated for the resulting p-values (FDR = 0.25). Ontologies with a BH-PV < 0.05 were considered statistically significant. In the case of highly similar ontology with significant changes, the ontology with the most proteins was selected to represent the results. The Python code used to analyze StringDB and calculate the FCs can be found in the GitHub repository JC-Price/PublicProteomeDataAnalysis: scripts for proteome data wrangling. https://github.com/JC-Price/PublicProteomeDataAnalysis

Supporting information

S1 File. Fig A. Detailed workflow chart describing both the mouse model and stages of analysis. Created with Biorender.com, Inkscape, Matplotlib.py, and Plotly.py. Fig B. Schematic of the minimum model for protein homeostasis applied to each protein Created with Inkscape, Matplotlib.py, and Plotly.py. Fig C. Abundance and turnover FCs for ontologies related to endolysosomal processes in A) E2vsE3 and B) E4vsE3 Created with Inkscape, Matplotlib.py, and Plotly.py. Fig D. Abundance and turnover FCs for ontologies related to mitochondrial components in A) E2vsE3 and B) E4vsE3 Created with Inkscape, Matplotlib.py, and Plotly.py. Fig E. Abundance and turnover FCs for ontologies related to cellular metabolism in A) E2vsE3 and B) E4vsE3 Created with Inkscape, Matplotlib.py, and Plotly.py. Fig F. Abundance and turnover FCs for ontologies related to protein degradation in A) E2vsE3 and B) E4vsE3 Created with Inkscape, Matplotlib.py, and Plotly.py. Fig G. Model for comparison of ApoE2-dependent changes between brain and liver. Created with Biorender.com and Inkscape. Fig H. Model for comparison of ApoE4-dependent changes between brain and liver. Created with Biorender.com and Inkscape.
(DOCX)

S1 Table. Organization of the mouse cohort used in this study created with Excel.
(XLSX)

S2 Table. Brain tissue protein information study created with Numpy.py and Pandas.py.
(XLSX)

S3 Table. Brain tissue protein information study created with Numpy.py and Pandas.py.
(XLSX)

S4 Table. Brain protein ontology grouping, fold changes, and statistics study created with Numpy.py and Pandas.py.
(XLSX)

S5 Table. Liver protein ontology grouping, fold changes, and statistics study created with Numpy.py and Pandas.py.
(XLSX)

Acknowledgments

The mice used in this research were provided by Johnathan J. Wisco, Ph. D. We gratefully acknowledge the support of BYU's live animal facility, Kevin Rey and the BYU Hydrology Laboratory, and the Fritz B. Burns Biological Mass Spectrometry Facility. Figures were created using Inkscape, Matplotlib.py, Biorender, and Plotly.py

Author Contributions

Conceptualization: Nathan R. Zuniga, John C. Price.

Data curation: Nathan R. Zuniga, Ariel E. A. Denos, John C. Price.

Formal analysis: Nathan R. Zuniga, Noah E. Earls, Ariel E. A. Denos, Jared M. Elison, Benjamin S. Jones, Chad D. Hyer, Mark K. Transtrum.

Funding acquisition: Haifa M. Almughamsi, John C. Price.

Investigation: Nathan R. Zuniga, Noah E. Earls, Ariel E. A. Denos, Jared M. Elison, Benjamin S. Jones, Ethan G. Smith, Noah G. Moran, Katie L. Broce, Gerome M. Romero, Kimberly B. Wagstaff, Haifa M. Almughamsi.

Methodology: Nathan R. Zuniga, Ariel E. A. Denos, Haifa M. Almughamsi, John C. Price.

Project administration: John C. Price.

Resources: John C. Price.

Software: Nathan R. Zuniga.

Supervision: Nathan R. Zuniga, Mark K. Transtrum, John C. Price.

Validation: Nathan R. Zuniga, Noah E. Earls, Ariel E. A. Denos, Benjamin S. Jones, Ethan G. Smith, Noah G. Moran, Katie L. Broce, Gerome M. Romero, Kimberly B. Wagstaff, Haifa M. Almughamsi, Mark K. Transtrum.

Visualization: Nathan R. Zuniga, Chad D. Hyer, John C. Price.

Writing – original draft: Nathan R. Zuniga, Noah E. Earls, Ethan G. Smith, Chad D. Hyer, Mark K. Transtrum.

Writing – review & editing: Noah E. Earls, Ariel E. A. Denos, Jared M. Elison, John C. Price.

References

1. Liu CC, Kanekiyo T, Xu H, Bu GJ. Apolipoprotein E and Alzheimer disease: risk, mechanisms and therapy (vol 9, pg 106, 2013). Nat Rev Neurol. 2013; 9(4):184–. https://doi.org/10.1038/nrneurol.2013.32 WOS:000317268100012.
2. Husain MA, Laurent B, Plourde M. APOE and Alzheimer's Disease: From Lipid Transport to Physiopathology and Therapeutics. Frontiers in Neuroscience. 2021;15. Epub 2021/02/17. https://doi.org/10.3389/fnins.2021.630502 PMID: 33679311; PubMed Central PMCID: PMC7925634.
3. Feussner G, Albanese M, Valencia A. Three-dimensional structure of the LDL receptor-binding domain of the human apolipoprotein E2 (Arg136—>Cys) variant. Atherosclerosis. 1996; 126(2):177–84. https://doi.org/10.1016/0021-9150(96)05870-4 PMID: 8902143.
4. Mahley RW. Central Nervous System Lipoproteins: ApoE and Regulation of Cholesterol Metabolism. Arterioscler Thromb Vasc Biol. 2016; 36(7):1305–15. Epub 2016/05/14. https://doi.org/10.1161/ATVBAHA.116.307023 PMID: 27174096; PubMed Central PMCID: PMC4942259.
5. Farrer LA, Cupples LA, Haines JL, Hyman B, Kukull WA, Mayeux R, et al. Effects of Age, Sex, and Ethnicity on the Association Between Apolipoprotein E Genotype and Alzheimer Disease: A Meta-analysis. JAMA. 1997; 278(16):1349–56. https://doi.org/10.1001/jama.1997.03550160069041
6. Breslow JL, Zannis VI, Sangiacomo TR, Third JLHC, Tracy T, Glueck CJ. Studies of Familial Type-Iii Hyperlipoproteinemia Using as a Genetic-Marker the Apoe Phenotype E2/2. J Lipid Res. 1982; 23(8):1224–35. Epub 2021/01/04. https://doi.org/10.1016/S0022-2275(20)38060-3 WOS:A1982PQ58200016.
7. Huang XM, Chen PC, Poole C. APOE-epsilon 2 allele associated with higher prevalence of sporadic Parkinson disease. Neurology. 2004; 62(12):2198–202. https://doi.org/10.1212/01.wnl.0000130159.28215.6a WOS:000222178600011. PMID: 15210882
8. Phillips MC. Apolipoprotein E Isoforms and Lipoprotein Metabolism. Iubmb Life. 2014; 66(9):616–23. https://doi.org/10.1002/iub.1314 WOS:000344160700003. PMID: 25328986
9. Kuo CL, Pilling LC, Atkins JL, Masoli JAH, Delgado J, Kuchel GA, et al. APOE e4 Genotype Predicts Severe COVID-19 in the UK Biobank Community Cohort. J Gerontol a-Biol. 2020; 75(11):2231–2. https://doi.org/10.1093/gerona/glaa131 WOS:000579870000030; PubMed Central PMCID: PMC PMC7314139. PMID: 32451547
10. Fagan AM, Watson M, Parsadanian M, Bales KR, Paul SM, Holtzman DM. Human and murine ApoE markedly alters A beta metabolism before and after plaque formation in a mouse model of Alzheimer's disease. Neurobiol Dis. 2002; 9(3):305–18. Epub 2002/04/13. https://doi.org/10.1006/nbdi.2002.0483 PMID: 11950276.
11. Fryer JD, Simmons K, Parsadanian M, Bales KR, Paul SM, Sullivan PM, et al. Human apolipoprotein E4 alters the amyloid-beta 40:42 ratio and promotes the formation of cerebral amyloid angiopathy in an amyloid precursor protein transgenic model. J Neurosci. 2005; 25(11):2803–10. Epub 2005/03/18. https://doi.org/10.1523/JNEUROSCI.5170-04.2005 PMID: 15772340; PubMed Central PMCID: PMC6725147.
12. Hunsberger HC, Pinky PD, Smith W, Suppiramaniam V, Reed MN. The role of APOE4 in Alzheimer's disease: strategies for future therapeutic interventions. Neuronal Signal. 2019; 3(2):NS20180203. Epub 20190418. https://doi.org/10.1042/NS20180203 PMID: 32269835; PubMed Central PMCID: PMC7104324.
13. Ji ZS, Miranda RD, Newhouse YM, Weisgraber KH, Huang Y, Mahley RW. Apolipoprotein E4 potentiates amyloid beta peptide-induced lysosomal leakage and apoptosis in neuronal cells. J Biol Chem. 2002; 277(24):21821–8. Epub 2002/03/26. https://doi.org/10.1074/jbc.M112109200 PMID: 11912196.
14. Tcw J, Qian L, Pipalia NH, Chao MJ, Liang SA, Shi Y, et al. Cholesterol and matrisome pathways dysregulated in astrocytes and microglia. Cell. 2022; 185(13):2213–33.e25. https://doi.org/10.1016/j.cell.2022.05.017 PMID: 35750033
15. Theendakara V, Peters-Libeu CA, Spilman P, Poksay KS, Bredesen DE, Rao RV. Direct Transcriptional Effects of Apolipoprotein E. J Neurosci. 2016; 36(3):685–700. https://doi.org/10.1523/JNEUROSCI.3562-15.2016 PMID: 26791201; PubMed Central PMCID: PMC4719010.
16. Zhou AL, Swaminathan SK, Curran GL, Poduslo JF, Lowe VJ, Li L, et al. Apolipoprotein A-I Crosses the Blood-Brain Barrier through Clathrin-Independent and Cholesterol-Mediated Endocytosis. J Pharmacol Exp Ther. 2019; 369(3):481–8. Epub 2019/04/12. https://doi.org/10.1124/jpet.118.254201 PMID: 30971477; PubMed Central PMCID: PMC6538888.
17. Qi GY, Mi YS, Shi XJ, Gu HW, Brinton RD, Yin F. ApoE4 Impairs Neuron-Astrocyte Coupling of Fatty Acid Metabolism. Cell Rep. 2021; 34(1). ARTN 108572 https://doi.org/10.1016/j.celrep.2020.108572 WOS:000605650500005. PMID: 33406436

18. Lumsden AL, Mulugeta A, Zhou A, Hypponen E. Apolipoprotein E (APOE) genotype-associated disease risks: a phenome-wide, registry-based, case-control study utilising the UK Biobank. EBioMedicine. 2020; 59:102954. Epub 2020/08/21. https://doi.org/10.1016/j.ebiom.2020.102954 PMID: 32818802; PubMed Central PMCID: PMC7452404.

19. Chou CJ, Affolter M, Kussmann M. A Nutrigenomics View of Protein Intake: Macronutrient, Bioactive Peptides, and Protein Turnover. In: Bouchard C, Ordovas JM, editors. Progress in Molecular Biology and Translational Science. 108: Academic Press; 2012. p. 51–74.

20. Hook V, Yoon M, Mosier C, Ito G, Podvin S, Head BP, et al. Cathepsin B in neurodegeneration of Alzheimer's disease, traumatic brain injury, and related brain disorders. Biochim Biophys Acta Proteins Proteom. 2020; 1868(8):140428. Epub 2020/04/20. https://doi.org/10.1016/j.bbapap.2020.140428 PMID: 32305689; PubMed Central PMCID: PMC7261628.

21. Schmukler E, Solomon S, Simonovitch S, Goldshmit Y, Wolfson E, Michaelson DM, et al. Altered mitochondrial dynamics and function in APOE4-expressing astrocytes. Cell Death & Disease. 2020; 11 (7):578. https://doi.org/10.1038/s41419-020-02776-4 PubMed Central PMCID: PMC7382473. PMID: 32709881

22. Area-Gomez E, Larrea D, Pera M, Agrawal RR, Guilfoyle DN, Pirhaji L, et al. APOE4 is Associated with Differential Regional Vulnerability to Bioenergetic Deficits in Aged APOE Mice. Sci Rep-Uk. 2020; 10(1). ARTN 4277 https://doi.org/10.1038/s41598-020-61142-8 WOS:000563338200001. PMID: 32152337

23. Fernández-Fernández MR, Gragera M, Ochoa-Ibarrola L, Quintana-Gallardo L, Valpuesta JM. Hsp70—a master regulator in protein degradation. FEBS Letters. 2017; 591(17):2648–60. Epub 2017/07/25. https://doi.org/10.1002/1873-3468.12751 PMID: 28696498.

24. Lin YT, Seo J, Gao F, Feldman HM, Wen HL, Penney J, et al. APOE4 Causes Widespread Molecular and Cellular Alterations Associated with Alzheimer's Disease Phenotypes in Human iPSC-Derived Brain Cell Types. Neuron. 2018; 98(6):1141–54.e7. Epub 2018/05/31. https://doi.org/10.1016/j.neuron.2018.05.008 PMID: 29861287; PubMed Central PMCID: PMC6023751.

25. Bonet-Costa V, Pomatto LC-D, Davies KJA. The Proteasome and Oxidative Stress in Alzheimer's Disease. Antioxidants & Redox Signaling. 2016; 25(16):886–901. https://doi.org/10.1089/ars.2016.6802 PMID: 27392670

26. Paradise V, Sabu M, Bafia J, Sharif NA, Nguyen C, Konrad-Vicario KD, et al. Dysregulation of neuroproteasomes by ApoE isoforms drives endogenous Tau aggregation. bioRxiv. 2023. https://doi.org/10.1101/2022.11.29.518293

27. Chen Y, Durakoglugil MS, Xian XD, Herz J. ApoE4 reduces glutamate receptor function and synaptic plasticity by selectively impairing ApoE receptor recycling. P Natl Acad Sci USA. 2010; 107 (26):12011–6. https://doi.org/10.1073/pnas.0914984107 WOS:000279332300064. PMID: 20547867

28. Dumanis SB, DiBattista AM, Miessau M, Moussa CE, Rebeck GW. APOE genotype affects the presynaptic compartment of glutamatergic nerve terminals. J Neurochem. 2013; 124(1):4–14. Epub 20120928. https://doi.org/10.1111/j.1471-4159.2012.07908.x PMID: 22862561; PubMed Central PMCID: PMC3509249.

29. Zhong N, Ramaswamy G, Weisgraber KH. Apolipoprotein E4 Domain Interaction Induces Endoplasmic Reticulum Stress and Impairs Astrocyte Function*. J Biol Chem. 2009; 284(40):27273–80. https://doi.org/10.1074/jbc.M109.014464 PMID: 19666463

30. Marcotti S, Sánchez-Sánchez BJ, Serna-Morales E, Dragu A, Díaz-de-la-Loza M-d-C, Matsubayashi Y, et al. Protocol for intervention-free quantification of protein turnover rate by steady-state modeling. STAR Protocols. 2021; 2(1). https://doi.org/10.1016/j.xpro.2021.100377 PubMed Central PMCID: PMC8102804. PMID: 33786460

31. Ross AB, Langer JD, Jovanovic M. Proteome Turnover in the Spotlight: Approaches, Applications, and Perspectives. Mol Cell Proteomics. 2021;20. Epub 2020/12/07. https://doi.org/10.1074/mcp.R120.002190 PMID: 33556866; PubMed Central PMCID: PMC7950106.

32. Waterlow JC, Waterlow JC. Protein turnover. Wallingford, UK; Cambridge, MA: CABI Pub.; 2006. x, 301 p. p.

33. Xian X, Pohlkamp T, Durakoglugil MS, Wong CH, Beck JK, Lane-Donovan C, et al. Reversal of ApoE4-induced recycling block as a novel prevention approach for Alzheimer's disease. Elife. 2018; 7: e40048. https://doi.org/10.7554/eLife.40048 PMID: 30375977

34. Nuriel T, Peng KY, Ashok A, Dillman AA, Figueroa HY, Apuzzo J, et al. The Endosomal–Lysosomal Pathway Is Dysregulated by APOE4 Expression in Vivo. Frontiers in Neuroscience. 2017;11.

35. Heeren J, Grewal T, Laatsch A, Becker N, Rinninger F, Rye KA, et al. Impaired recycling of apolipoprotein E4 is associated with intracellular cholesterol accumulation. J Biol Chem. 2004; 279(53):55483–92. https://doi.org/10.1074/jbc.M409324200 WOS:000225960800063. PMID: 15485881

36. Bonifacino JS, Glick BS. The mechanisms of vesicle budding and fusion. Cell. 2004; 116(2):153–66. https://doi.org/10.1016/s0092-8674(03)01079-1 PMID: 14744428.

37. Lin RC, Scheller RH. Mechanisms of synaptic vesicle exocytosis. Annual Review of Cell and Developmental Biology. 2000; 16:19–49. https://doi.org/10.1146/annurev.cellbio.16.1.19 PMID: 11031229.

38. Narayan P, Sienski G, Bonner JM, Lin YT, Seo J, Baru V, et al. PICALM Rescues Endocytic Defects Caused by the Alzheimer's Disease Risk Factor APOE4. Cell Rep. 2020; 33(1). https://doi.org/10.1016/j.celrep.2020.108224 PMID: 33027662; PubMed Central PMCID: PMC8190562.

39. Ando K, Nagaraj S, Küçükali F, de Fisenne M-A, Kosa A-C, Doeraene E, et al. PICALM and Alzheimers Disease: An Update and Perspectives. Cells. 2022; 11(24). https://doi.org/10.3390/cells11243994 PMID: 36552756

40. Yang C, Wang X. Lysosome biogenesis: Regulation and functions. Journal of Cell Biology. 2021; 220 (6). https://doi.org/10.1083/jcb.202102001 PubMed Central PMCID: PMC8105738. PMID: 33950241

41. de Leeuw SM, Kirschner AWT, Lindner K, Rust R, Budny V, Wolski WE, et al. APOE2, E3, and E4 differentially modulate cellular homeostasis, cholesterol metabolism, and inflammatory response in isogenic iPSC-derived astrocytes. Stem Cell Reports. 2022; 17(1):110–26. https://doi.org/10.1016/j.stemcr.2021.11.007 PMID: 34919811

42. Giorgi C, Marchi S, Pinton P. The machineries, regulation and cellular functions of mitochondrial calcium. Nature Reviews Molecular Cell Biology. 2018; 19(11):713–30. https://doi.org/10.1038/s41580-018-0052-8 PMID: 30143745.

43. Calvo-Rodriguez M, Bacskai BJ. Mitochondria and Calcium in Alzheimer's Disease: From Cell Signaling to Neuronal Cell Death. Trends in Neurosciences. 2021; 44(2):136–51. https://doi.org/10.1016/j.tins.2020.10.004 PMID: 33160650

44. Mahley RW. Apolipoprotein E4 targets mitochondria and the mitochondria-associated membrane complex in neuropathology, including Alzheimer's disease. Current Opinion in Neurobiology. 2023; 79:102684. https://doi.org/10.1016/j.conb.2023.102684 PMID: 36753858

45. Rath S, Sharma R, Gupta R, Ast T, Chan C, Durham TJ, et al. MitoCarta3.0: an updated mitochondrial proteome now with sub-organelle localization and pathway annotations. Nucleic Acids Research. 2021; 49(D1):D1541–D7. https://doi.org/10.1093/nar/gkaa1011 PubMed Central PMCID: PMC7778944. PMID: 33174596

46. Mick David U, Dennerlein S, Wiese H, Reinhold R, Pacheu-Grau D, Lorenzi I, et al. MITRAC Links Mitochondrial Protein Translocation to Respiratory-Chain Assembly and Translational Regulation. Cell. 2012; 151(7):1528–41. https://doi.org/10.1016/j.cell.2012.11.053 PMID: 23260140

47. Aiyar RS, Bohnert M, Duvezin-Caubet S, Voisset C, Gagneur J, Fritsch ES, et al. Mitochondrial protein sorting as a therapeutic target for ATP synthase disorders. Nature Communications. 2014;5(1). https://doi.org/10.1038/ncomms6585 PubMed Central PMCID: PMC4284804. PMID: 25519239

48. Anand R, Reichert AS, Kondadi AK. Emerging Roles of the MICOS Complex in Cristae Dynamics and Biogenesis. Biology. 2021;10(7). https://doi.org/10.3390/biology10070600 PMID: 34209580

49. van der Laan M, Horvath SE, Pfanner N. Mitochondrial contact site and cristae organizing system. Current Opinion in Cell Biology. 2016; 41:33–42. https://doi.org/10.1016/j.ceb.2016.03.013 PMID: 27062547

50. Xinglong W, Bo S, Hyoung-gon L, Xinyi L, George P, Mark AS, et al. Impaired Balance of Mitochondrial Fission and Fusion in Alzheimer's Disease. The Journal of Neuroscience. 2009; 29(28):9090–103. https://doi.org/10.1523/JNEUROSCI.1357-09.2009. PubMed Central PMCID: PMC2735241. PMID: 19605646

51. Schon EA, Area-Gomez E. Mitochondria-associated ER membranes in Alzheimer disease. Molecular and Cellular Neuroscience. 2013; 55:26–36. https://doi.org/10.1016/j.mcn.2012.07.011 PMID: 22922446

52. Schon Eric A, Przedborski S. Mitochondria: The Next (Neurode)Generation. Neuron. 2011; 70 (6):1033–53. https://doi.org/10.1016/j.neuron.2011.06.003 PMID: 21689593

53. Nakamura T, Watanabe A, Fujino T, Hosono T, Michikawa M. Apolipoprotein E4 (1–272) fragment is associated with mitochondrial proteins and affects mitochondrial function in neuronal cells. Molecular Neurodegeneration. 2009; 4(1):35. https://doi.org/10.1186/1750-1326-4-35 PMID: 19695092

54. Williams HC, Farmer BC, Piron MA, Walsh AE, Bruntz RC, Gentry MS, et al. APOE alters glucose flux through central carbon pathways in astrocytes. Neurobiology of Disease. 2020; 136. https://doi.org/10.1016/j.nbd.2020.104742 WOS:000516662200023; PubMed Central PMCID: PMC7044721. PMID: 31931141

55. Orr AL, Kim C, Jimenez-Morales D, Newton BW, Johnson JR, Krogan NJ, et al. Neuronal Apolipoprotein E4 Expression Results in Proteome-Wide Alterations and Compromises Bioenergetic Capacity by

Disrupting Mitochondrial Function. Journal of Alzheimer's Disease. 2019; 68:991–1011. https://doi.org/10.3233/JAD-181184 PubMed Central PMCID: PMC6481541. PMID: 30883359

56. Brandon CF, Holden CW, Nicholas D, Margaret AP, Grant KN, David JC, et al. APOE4 Lowers Energy Expenditure and Impairs Glucose Oxidation by Increasing Flux through Aerobic Glycolysis. Molecular Neurodegeneration. 2020; 16. Epub 2021/09/06. https://doi.org/10.1186/s13024-021-00483-y PMID: 34488832

57. Zhang X, Wu L, Swerdlow RH, Zhao L. Opposing Effects of ApoE2 and ApoE4 on Glycolytic Metabolism in Neuronal Aging Supports a Warburg Neuroprotective Cascade against Alzheimer's Disease. Cells. 2023; 12(3). Epub 20230125. https://doi.org/10.3390/cells12030410 PMID: 36766752; PubMed Central PMCID: PMC9914046.

58. Valla J, Yaari R, Wolf AB, Kusne Y, Beach TG, Roher AE, et al. Reduced Posterior Cingulate Mitochondrial Activity in Expired Young Adult Carriers of the APOE ε4 Allele, the Major Late-Onset Alzheimer's Susceptibility Gene. Journal of Alzheimer's Disease. 2010; 22(1):307–13. https://doi.org/10.3233/JAD-2010-100129 PubMed Central PMCID: PMC3124564. PMID: 20847408

59. Long W, Xin Z, Liqin Z. Human ApoE Isoforms Differentially Modulate Brain Glucose and Ketone Body Metabolism: Implications for Alzheimer's Disease Risk Reduction and Early Intervention. J Neurosci. 2018;38(30):6665–81. https://doi.org/10.1523/JNEUROSCI.2262-172018.

60. Small GW, Ercoli LM, Silverman DHS, Huang SC, Komo S, Bookheimer SY, et al. Cerebral metabolic and cognitive decline in persons at genetic risk for Alzheimer's disease. Proceedings of the National Academy of Sciences. 2000; 97(11):6037–42. https://doi.org/10.1073/pnas.090106797 WOS:000087318700066. PMID: 10811879

61. Wu L, Zhang X, Zhao L. Human ApoE Isoforms Differentially Modulate Brain Glucose and Ketone Body Metabolism: Implications for Alzheimer's Disease Risk Reduction and Early Intervention. J Neurosci. 2018; 38(30):6665–81. Epub 2018/07/02. https://doi.org/10.1523/JNEUROSCI.2262-17.2018 PMID: 29967007; PubMed Central PMCID: PMC6067075.

62. Chin D, Hagl S, Hoehn A, Huebbe P, Pallauf K, Grune T, et al. Adenosine triphosphate concentrations are higher in the brain of APOE3- compared to APOE4-targeted replacement mice and can be modulated by curcumin. Genes & Nutrition. 2014; 9(3). Epub 2014/03/27. https://doi.org/10.1007/s12263-014-0397-3 PMID: 24671632; PubMed Central PMCID: PMC4026431.

63. Yin J, Nielsen M, Carcione T, Li S, Shi J. Apolipoprotein E regulates mitochondrial function through the PGC-1α-sirtuin 3 pathway. Aging (Albany NY). 2019; 11(23):11148–56. Epub 2019/12/06. https://doi.org/10.18632/aging.102516 PMID: 31808750; PubMed Central PMCID: PMC6932918.

64. Fang W, Xiao N, Zeng G, Bi D, Dai X, Mi X, et al. APOE4 genotype exacerbates the depression-like behavior of mice during aging through ATP decline. Translational Psychiatry. 2021; 11(1). https://doi.org/10.1038/s41398-021-01631-0 PubMed Central PMCID: PMC8492798. PMID: 34611141

65. Kodroń A, Mussulini BH, Pilecka I, Chacińska A. The ubiquitin-proteasome system and its crosstalk with mitochondria as therapeutic targets in medicine. Pharmacol Res. 2021;163. https://doi.org/10.1016/j.phrs.2020.105248 PMID: 33065283

66. Mishra R, Upadhyay A, Prajapati VK, Mishra A. Proteasome-mediated proteostasis: Novel medicinal and pharmacological strategies for diseases. Medicinal Research Reviews. 2018; 38(6):1916–73. https://doi.org/10.1002/med.21502 PMID: 29719055

67. Wang F, Durfee LA, Huibregtse JM. A cotranslational ubiquitination pathway for quality control of misfolded proteins. Mol Cell. 2013; 50(3):368–78. Epub 2013/04/16. https://doi.org/10.1016/j.molcel.2013.03.009 PMID: 23583076; PubMed Central PMCID: PMC3654026.

68. Song JY, Wang XG, Zhang ZY, Che L, Fan B, Li GY. Endoplasmic reticulum stress and the protein degradation system in ophthalmic diseases. Peerj. 2020; 8. ARTN e8638 https://doi.org/10.7717/peerj.8638 WOS:000514681600007. PMID: 32117642

69. Hou X, Zhang X, Zou H, Guan M, Fu C, Wang W, et al. Differential and substrate-specific inhibition of γ-secretase by the C-terminal region of ApoE2, ApoE3, and ApoE4. Neuron. 2023; 111(12):1898–913.e5. https://doi.org/10.1016/j.neuron.2023.03.024 PMID: 37040764

70. Dorey E, Bamji-Mirza M, Najem D, Li Y, Liu H, Callaghan D, et al. Apolipoprotein E Isoforms Differentially Regulate Alzheimer's Disease and Amyloid-β-Induced Inflammatory Response in vivo and in vitro. Journal of Alzheimer's Disease. 2017; 57(4):1265–79. https://doi.org/10.3233/JAD-160133 PMID: 28372324

71. He K, Nie L, Zhou Q, Rahman SU, Liu J, Yang X, et al. Proteomic Profiles of the Early Mitochondrial Changes in APP/PS1 and ApoE4 Transgenic Mice Models of Alzheimer's Disease. Journal of Proteome Research. 2019; 18(6):2632–42. Epub 2019/05/13. https://doi.org/10.1021/acs.jproteome.9b00136 PMID: 31055927

72. Miyata M, Smith JD. Apolipoprotein E allele–specific antioxidant activity and effects on cytotoxicity by oxidative insults and β–amyloid peptides. Nature Genetics. 1996; 14(1):55–61. https://doi.org/10.1038/ng0996-55 PMID: 8782820

73. Thibaudeau TA, Anderson RT, Smith DM. A common mechanism of proteasome impairment by neurodegenerative disease-associated oligomers. Nature Communications. 2018; 9(1):1097. https://doi.org/10.1038/s41467-018-03509-0 PMID: 29545515

74. Tseng BP, Green KN, Chan JL, Blurton-Jones M, LaFerla FM. Aβ inhibits the proteasome and enhances amyloid and tau accumulation. Neurobiology of Aging. 2008; 29(11):1607–18. Epub 2007/06/01. https://doi.org/10.1016/j.neurobiolaging.2007.04.014 PMID: 17544172

75. Wang X, Yen J, Kaiser P, Huang L. Regulation of the 26S Proteasome Complex During Oxidative Stress. Science Signaling. 2010; 3(151):ra88. https://doi.org/10.1126/scisignal.2001232 PMID: 21139140

76. Ross JM, Olson L, Coppotelli G. Mitochondrial and Ubiquitin Proteasome System Dysfunction in Ageing and Disease: Two Sides of the Same Coin? International Journal of Molecular Sciences [Internet]. 2015; 16(8):[19458–76 pp.]. https://doi.org/10.3390/ijms160819458 PMID: 26287188

77. Dambacher CM, Worden EJ, Herzik MA, Jr., Martin A, Lander GC. Atomic structure of the 26S proteasome lid reveals the mechanism of deubiquitinase inhibition. Elife. 2016; 5. https://doi.org/10.7554/eLife.13027 PMID: 26744777

78. Fote GM, Geller NR, Efstathiou NE, Hendricks N, Vavvas DG, Reidling JC, et al. Isoform-dependent lysosomal degradation and internalization of apolipoprotein E requires autophagy proteins. Journal of Cell Science. 2022;135(2). Epub 2022/01/25. https://doi.org/10.1242/jcs.258687 PMID: 34982109; PubMed Central PMCID: PMC8917355.

79. Burger B, Vaudel M, Barsnes H. Importance of Block Randomization When Designing Proteomics Experiments. J Proteome Res. 2021; 20(1):122–8. Epub 2020/09/25. https://doi.org/10.1021/acs.jproteome.0c00536 PMID: 32969222; PubMed Central PMCID: PMC7786377.

80. Szklarczyk D, Gable AL, Lyon D, Junge A, Wyder S, Huerta-Cepas J, et al. STRING v11: protein-protein association networks with increased coverage, supporting functional discovery in genome-wide experimental datasets. Nucleic Acids Res. 2019; 47(D1):D607–D13. Epub 2018/11/27. https://doi.org/10.1093/nar/gky1131 PMID: 30476243; PubMed Central PMCID: PMC6323986.

81. Andersen JS, Lam YW, Leung AK, Ong SE, Lyon CE, Lamond AI, et al. Nucleolar proteome dynamics. Nature. 2005; 433(7021):77–83. Epub 2005/01/07. https://doi.org/10.1038/nature03207 PMID: 15635413.

82. Kuechler ER, Budzynska PM, Bernardini JP, Gsponer J, Mayor T. Distinct Features of Stress Granule Proteins Predict Localization in Membraneless Organelles. J Mol Biol. 2020; 432(7):2349–68. Epub 2020/02/28. https://doi.org/10.1016/j.jmb.2020.02.020 PMID: 32105731.

83. Buccitelli C, Selbach M. mRNAs, proteins and the emerging principles of gene expression control. Nat Rev Genet. 2020; 21(10):630–44. Epub 2020/07/28. https://doi.org/10.1038/s41576-020-0258-4 PMID: 32709985.

84. Martin-Perez M, Villen J. Determinants and Regulation of Protein Turnover in Yeast. Cell Syst. 2017; 5(3):283–94 e5. Epub 2017/09/18. https://doi.org/10.1016/j.cels.2017.08.008 PMID: 28918244; PubMed Central PMCID: PMC5935796.

85. Schwanhausser B, Busse D, Li N, Dittmar G, Schuchhardt J, Wolf J, et al. Global quantification of mammalian gene expression control. Nature. 2011; 473(7347):337–42. Epub 2011/05/20. https://doi.org/10.1038/nature10098 PMID: 21593866.

86. Mathis AD, Naylor BC, Carson RH, Evans E, Harwell J, Knecht J, et al. Mechanisms of In Vivo Ribosome Maintenance Change in Response to Nutrient Signals. Mol Cell Proteomics. 2017; 16(2):243–54. Epub 2016/12/10. https://doi.org/10.1074/mcp.M116.063255 PMID: 27932527; PubMed Central PMCID: PMC5294211.

87. Price JC, Guan S, Burlingame A, Prusiner SB, Ghaemmaghami S. Analysis of proteome dynamics in the mouse brain. Proc Natl Acad Sci U S A. 2010; 107(32):14508–13. Epub 2010/08/12. https://doi.org/10.1073/pnas.1006551107 PMID: 20699386; PubMed Central PMCID: PMC2922600.

88. McShane E, Sin C, Zauber H, Wells JN, Donnelly N, Wang X, et al. Kinetic Analysis of Protein Stability Reveals Age-Dependent Degradation. Cell. 2016; 167(3):803–15 e21. Epub 2016/10/22. https://doi.org/10.1016/j.cell.2016.09.015 PMID: 27720452.

89. Meadow ME, Broas S, Hoare M, Alimohammadi F, Welle KA, Swovick K, et al. Proteome Birthdating Reveals Age-Selectivity of Protein Ubiquitination. Mol Cell Proteomics. 2024; 23(7):100791. Epub 2024/05/27. https://doi.org/10.1016/j.mcpro.2024.100791 PMID: 38797438.

90. Iizuka R, Yamagishi-Shirasaki M, Funatsu T. Kinetic study of de novo chromophore maturation of fluorescent proteins. Analytical Biochemistry. 2011; 414(2):173–8. Epub 2011/04/01. https://doi.org/10.1016/j.ab.2011.03.036 PMID: 21459075.

91. Beynon RJ. The dynamics of the proteome: strategies for measuring protein turnover on a proteome-wide scale. Briefings in Functional Genomics. 2005; 3(4):382–90. https://doi.org/10.1093/bfgp/3.4.382 PMID: 15814028.

92. Dörrbaum AR, Kochen L, Langer JD, Schuman EM. Local and global influences on protein turnover in neurons and glia. Elife. 2018;7. https://doi.org/10.7554/eLife.34202 PubMed Central PMCID: PMC6008053. PMID: 29914620

93. Dhondt I, Petyuk VA, Bauer S, Brewer HM, Smith RD, Depuydt G, et al. Changes of Protein Turnover in Aging Caenorhabditis elegans. Molecular and Cellular Proteomics. 2017; 16(9):1621–33. Epub 2017/07/05. https://doi.org/10.1074/mcp.RA117.000049 PMID: 28679685; PubMed Central PMCID: PMC5587862.

94. Visscher M, De Henau S, Wildschut Mattheus HE, van Es Robert M, Dhondt I, Michels H, et al. Proteome-wide Changes in Protein Turnover Rates in C. elegans Models of Longevity and Age-Related Disease. Cell Rep. 2016; 16(11):3041–51. https://doi.org/10.1016/j.celrep.2016.08.025 PMID: 27626671

95. Jonathon JOB, Vikram N, Yao W, Phillip S, Celeste MS, Nicole H, et al. Precise Estimation of In Vivo Protein Turnover Rates. bioRxiv. 2020. https://doi.org/10.1101/2020.11.10.377440

96. Claydon AJ, Beynon R. Proteome Dynamics: Revisiting Turnover with a Global Perspective. Molecular & Cellular Proteomics. 2012; 11(12):1551–65. Epub 2012/11/02. https://doi.org/10.1074/mcp.O112.022186 WOS:000313557000004; PubMed Central PMCID: PMC3518130. PMID: 23125033

97. Miller BF, Reid JJ, Price JC, Lin HL, Atherton PJ, Smith K. CORP: The use of deuterated water for the measurement of protein synthesis. J Appl Physiol (1985). 2020; 128(5):1163–76. Epub 2020/03/28. https://doi.org/10.1152/japplphysiol.00855.2019 PMID: 32213116.

98. Naylor BC, Anderson CNK, Hadfield M, Parkinson DH, Ahlstrom A, Hannemann A, et al. Utilizing Non-equilibrium Isotope Enrichments to Dramatically Increase Turnover Measurement Ranges in Single Biopsy Samples from Humans. J Proteome Res. 2022; 21(11):2703–14. Epub 2022/09/14. https://doi.org/10.1021/acs.jproteome.2c00380 PMID: 36099490; PubMed Central PMCID: PMC9639613.

99. Black E, Rasch A, Wimmer T, Li A, Araujo A, Cieslak S, et al. The effects of age, genotype and diet on hippocampal subfield iron dysregulation and Alzheimer's disease biomarkers in an ApoE mouse model. European Journal of Neuroscience. 2023; 57(6):1033–47. https://doi.org/10.1111/ejn.15933 PMID: 36775930

100. Xu J, He K, Zhang K, Yang C, Nie L, Dan D, et al. Low-Dose Copper Exposure Exacerbates Depression-Like Behavior in ApoE4 Transgenic Mice. Oxidative Medicine and Cellular Longevevity. 2021; 2021:1–20. Epub 20210325. https://doi.org/10.1155/2021/6634181 PMID: 33833851; PubMed Central PMCID: PMC8018851.

101. Cieslak SG. The effects of L-Cysteine on Alzheimer's disease pathology in APOE2, APOE3, and APOE4 homozygous mice. Journal of Biomedical Nanotechnology. 2020;5. https://doi.org/10.15761/JBN.1000128

102. Chaudhari K, Wong JM, Vann PH, Como T, O'Bryant SE, Sumien N. ApoE Genotype-Dependent Response to Antioxidant and Exercise Interventions on Brain Function. Antioxidants (Basel). 2020; 9(6). Epub 2020/06/25. https://doi.org/10.3390/antiox9060553 PMID: 32630431; PubMed Central PMCID: PMC7346214.

103. Adhikari R, Steed KS, Hutchinson B, Wang H, Mendoza M, Staudte R, et al. Hippocampal T2 signal loss and decreased radial arm maze performance in transgenic murine model for AD. Brain Nerves. 2020; 5:1–8. https://doi.org/10.15761/JBN.1000127

104. Pandey RS, Graham L, Uyar A, Preuss C, Howell GR, Carter GW. Genetic perturbations of disease risk genes in mice capture transcriptomic signatures of late-onset Alzheimer's disease. Molecular Neurodegeneration. 2019; 14(1):50. https://doi.org/10.1186/s13024-019-0351-3 PMID: 31878951

105. Meng F-T, Zhao J, Fang H, Zhang L-F, Wu H-M, Liu Y-J. Upregulation of Mineralocorticoid Receptor in the Hypothalamus Associated with a High Anxiety-like Level in Apolipoprotein E4 Transgenic Mice. Behavior Genetics. 2017; 47(4):416–24. https://doi.org/10.1007/s10519-017-9843-5 PMID: 28337631

106. Jankowsky JL, Zheng H. Practical considerations for choosing a mouse model of Alzheimer's disease. Molecular Neurodegeneration. 2017; 12(1). https://doi.org/10.1186/s13024-017-0231-7 PubMed Central PMCID: PMC5741956. PMID: 29273078

107. Chaudhari K, Wong JM, Vann PH, Sumien N. Exercise, but not antioxidants, reversed ApoE4-associated motor impairments in adult GFAP-ApoE mice. Behavioural Brain Research. 2016; 305:37–45. https://doi.org/10.1016/j.bbr.2016.02.014 PMID: 26892275

108. Meng F-T, Zhao J, Fang H, Liu Y-J. The influence of chronic stress on anxiety-like behavior and cognitive function in different human GFAP-ApoE transgenic adult male mice. Stress. 2015; 18(4):419–26. https://doi.org/10.3109/10253890.2015.1040986 PMID: 25938810

109. Liao F, Zhang TJ, Jiang H, Lefton KB, Robinson GO, Vassar R, et al. Murine versus human apolipoprotein E4: differential facilitation of and co-localization in cerebral amyloid angiopathy and amyloid

plaques in APP transgenic mouse models. Acta Neuropathol Commun. 2015; 3:70. Epub 2015/11/12. https://doi.org/10.1186/s40478-015-0250-y PMID: 26556230; PubMed Central PMCID: PMC4641345.

110. Naylor BC, Porter MT, Wilson E, Herring A, Lofthouse S, Hannemann A, et al. DeuteRater: a tool for quantifying peptide isotope precision and kinetic proteomics. Bioinformatics. 2017; 33(10):1514–20. https://doi.org/10.1093/bioinformatics/btx009 PMID: 28093409.

111. Aguilan JT, Kulej K, Sidoli S. Guide for protein fold change and p-value calculation for non-experts in proteomics. Mol Omics. 2020; 16(6):573–82. Epub 20200924. https://doi.org/10.1039/d0mo00087f PMID: 32968743.

112. Pedregosa F, Varoquaux G, Gramfort A, Michel V, Thirion B, Grisel O, et al. Scikit-learn: Machine Learning in Python. J Mach Learn Res. 2011; 12:2825–30. https://doi.org/10.5555/1953048.2078195 WOS:000298103200003.

113. Virtanen P, Gommers R, Oliphant TE, Haberland M, Reddy T, Cournapeau D, et al. SciPy 1.0: fundamental algorithms for scientific computing in Python. Nature Methods. 2020; 17(3):261–72. https://doi.org/10.1038/s41592-019-0686-2 PubMed Central PMCID: PMC7056644. PMID: 32015543

114. van den Berg RA, Hoefsloot HC, Westerhuis JA, Smilde AK, van der Werf MJ. Centering, scaling, and transformations: improving the biological information content of metabolomics data. BMC Genomics. 2006; 7. Epub 2006/06/08. https://doi.org/10.1186/1471-2164-7-142 PMID: 16762068; PubMed Central PMCID: PMC1534033.

115. Price JC, Khambatta CF, Li KW, Bruss MD, Shankaran M, Dalidd M, et al. The effect of long term calorie restriction on in vivo hepatic proteostatis: a novel combination of dynamic and quantitative proteomics. Mol Cell Proteomics. 2012; 11(12):1801–14. Epub 2012/09/18. https://doi.org/10.1074/mcp.M112.021204 PMID: 22984287; PubMed Central PMCID: PMC3518108 and M. K. H. have a financial interest in KineMed Inc.

116. Price JC, Holmes WE, Li KW, Floreani NA, Neese RA, Turner SM, et al. Measurement of human plasma proteome dynamics with (2)H(2)O and liquid chromatography tandem mass spectrometry. Anal Biochem. 2012; 420(1):73–83. Epub 2011/10/04. https://doi.org/10.1016/j.ab.2011.09.007 PMID: 21964502.

117. Carson RH, Lewis CR, Erickson MN, Zagieboylo AP, Naylor BC, Li KW, et al. Imaging regiospecific lipid turnover in mouse brain with desorption electrospray ionization mass spectrometry. J Lipid Res. 2017; 58(9):1884–92. Epub 2017/07/27. https://doi.org/10.1194/jlr.M078170 PMID: 28743728; PubMed Central PMCID: PMC5580901.

118. Perez-Riverol Y, Csordas A, Bai J, Bernal-Llinares M, Hewapathirana S, Kundu DJ, et al. The PRIDE database and related tools and resources in 2019: improving support for quantification data. Nucleic Acids Research. 2019; 47(D1):D442–D50. https://doi.org/10.1093/nar/gky1106 PMID: 30395289; PubMed Central PMCID: PMC6323896.